



Investigation of Adaptive Control Approaches to Mitigate Shock Impact With Piezoceramics (Armor)

by Marthinus van Schoor and Jacob Pretorius

ARL-CR-0581

November 2006

prepared by

**Midé Technology Corporation
200 Boston Avenue Suite 1000
Medford, MA 02155**

under contract

DAAD-19-02-D-001

NOTICES

Disclaimers

The findings in this report are not to be construed as an official Department of the Army position unless so designated by other authorized documents.

Citation of manufacturer's or trade names does not constitute an official endorsement or approval of the use thereof.

DESTRUCTION NOTICE—Destroy this report when it is no longer needed. Do not return it to the originator.

Army Research Laboratory

Aberdeen Proving Ground, MD 21005-5069

ARL-CR-0581

November 2006

Investigation of Adaptive Control Approaches to Mitigate Shock Impact With Piezoceramics (Armor)

**by Marthinus van Schoor and Jacob Pretorius
Midé Technology Corporation**

prepared by

**Midé Technology Corporation
200 Boston Avenue Suite 1000
Medford, MA 02155**

under contract

DAAD-19-02-D-001

REPORT DOCUMENTATION PAGE			Form Approved OMB No. 0704-0188	
Public reporting burden for this collection of information is estimated to average 1 hour per response, including the time for reviewing instructions, searching existing data sources, gathering and maintaining the data needed, and completing and reviewing the collection information. Send comments regarding this burden estimate or any other aspect of this collection of information, including suggestions for reducing the burden, to Department of Defense, Washington Headquarters Services, Directorate for Information Operations and Reports (0704-0188), 1215 Jefferson Davis Highway, Suite 1204, Arlington, VA 22202-4302. Respondents should be aware that notwithstanding any other provision of law, no person shall be subject to any penalty for failing to comply with a collection of information if it does not display a currently valid OMB control number.				
PLEASE DO NOT RETURN YOUR FORM TO THE ABOVE ADDRESS.				
1. REPORT DATE (DD-MM-YYYY) November 2006		2. REPORT TYPE Final		3. DATES COVERED (From - To) July 2004 to April 2005
4. TITLE AND SUBTITLE Investigation of Adaptive Control Approaches to Mitigate Shock Impact With Piezoceramics (Armor)			5a. CONTRACT NUMBER	
			5b. GRANT NUMBER	
			5c. PROGRAM ELEMENT NUMBER	
6. AUTHOR(S) Marthinus van Schoor and Jacob Pretorius (both of Midé)			5d. PROJECT NUMBER 622618H80	
			5e. TASK NUMBER	
			5f. WORK UNIT NUMBER	
7. PERFORMING ORGANIZATION NAME(S) AND ADDRESS(ES) Midé Technology Corporation 200 Boston Avenue Suite 1000 Medford, MA 02155			8. PERFORMING ORGANIZATION REPORT NUMBER ARL-CR-0581	
9. SPONSORING/MONITORING AGENCY NAME(S) AND ADDRESS(ES) U.S. Army Research Laboratory Weapons and Materials Research Directorate Aberdeen Proving Ground, MD 21005-5066			10. SPONSOR/MONITOR'S ACRONYM(S)	
			11. SPONSOR/MONITOR'S REPORT NUMBER(S)	
12. DISTRIBUTION/AVAILABILITY STATEMENT Approved for public release; distribution is unlimited.				
13. SUPPLEMENTARY NOTES The contracting officer's representative (COR) is Tyrone Jones, U.S. Army Research Laboratory, ATTN: AMSRD-ARL-WM-TA, Aberdeen Proving Ground, MD 21005-5066, telephone number (410) 278-6223.				
14. ABSTRACT The U.S. Army Research Laboratory sought a Short-Term Analysis Services (STAS) program funded through Army Research Office (ARO) with Midé in the research, design, and development of an adaptive control system to mitigate the shock wave impact on an isolation system during and after a ballistic event. This report documents the initial work performed by Midé.				
15. SUBJECT TERMS adaptive control; armor; piezoceramics; shock mitigation				
16. SECURITY CLASSIFICATION OF:			17. LIMITATION OF ABSTRACT SAR	18. NUMBER OF PAGES 60
a. REPORT UNCLASSIFIED	b. ABSTRACT UNCLASSIFIED	c. THIS PAGE UNCLASSIFIED		
			19b. TELEPHONE NUMBER (Include area code) 410-278-6223	

Contents

List of Figures	iv
List of Tables	v
Acknowledgments	vi
Executive Summary	1
1. Description of Work Completed During Phase I	3
1.1 Task 1: Develop and Understand Requirements	3
1.1.1 Kick-off Meeting	3
1.1.2 Test Setup for Preliminary Tests	4
1.1.3 Preliminary Test Definitions	4
1.2 Task 2: Parametric Modeling	5
1.3 Task 3: Absorber Optimization	10
1.3.1 Finite Element Model Formulation	10
1.3.2 Anisotropic Materials	11
1.3.3 Modeling of Piezoelectric Materials	13
1.3.4 Linear Results	15
1.3.5 ANSYS Finite Element Model	20
1.4 Task 4: Preliminary Experiments	26
1.4.1 Kevlar Plate Tests	26
1.4.2 Integrated Piezo Tests	31
1.5 Task 5: Shock Absorber Design	36
2. Conclusion and Future Work	38
3. References	39
Appendix A. MATLAB Main Code	41
Distribution List	47

List of Figures

Figure 1. Finite element model.....	6
Figure 2. First non-rigid resonant mode shape.	6
Figure 3. Second non-rigid resonant mode shape.....	7
Figure 4. Third non-rigid resonant mode shape.....	7
Figure 5. Von Mises stress at 0.8 μ s after the 1.56-gram projectile impacted the center of the plate at 450 m/s	8
Figure 6. Von Mises stress at 4 μ s after the 1.56-gram projectile impacted the center of the plate at 450 m/s	8
Figure 7. Von Mises stress at 8 μ s after the 1.56-gram projectile impacted the center of the plate at 450 m/s	9
Figure 8. Displacement and velocity (deformation) of impact point.....	9
Figure 9. Displacement and velocity (deformation) of top surface directly above the impact point.	10
Figure 10. Deformation of a piezo cube when a voltage is applied across the d_{33} (Z-) direction	15
Figure 11. First mode shape of the ceramic-GRP composite target predicted by the Midé code.....	16
Figure 12. Displacement and velocity (deformation) of impact point.....	16
Figure 13. Displacement and velocity (deformation) of the top surface directly above the impact point	17
Figure 14. Predicted von Mises stresses at 230 microseconds after impact	17
Figure 15. First mode shape of the ceramic-GRP composite target predicted by the Midé code.....	18
Figure 16. Displacement and velocity (deformation) of impact point.....	18
Figure 17. Displacement and velocity (deformation) of the top surface directly above the impact point	19
Figure 18. Predicted von Mises Stresses at 230 micro-seconds after impact	19
Figure 19. The meshed ANSYS model.....	21
Figure 20. A typical result from the ANSYS analysis illustrating the nodal displacement in the z direction.....	21
Figure 21. Comparison of high speed video and the ANSYS model.	22
Figure 22. Voltage output from the PA1 piezo sensor during the ballistic test.	25
Figure 23. Voltage output from the PA1 piezo sensor in the ANSYS simulation.....	26
Figure 24. Kevlar displacement test setup.	27
Figure 25. Test setup as viewed from the gun barrel.....	27

Figure 26. The gun, left and side view of the eddy gauge, metal strip and Kevlar target, right.....	28
Figure 27. Setup before test number 2646.....	29
Figure 28. Failure during test 2646.....	29
Figure 29. Failure of test 2647.....	30
Figure 30. The impact point is well above the position of the 075-inch metal disk in test 2648.....	30
Figure 31. Delaminating of the 0.75-inch metal disk during test 2649.....	31
Figure 32. Failure of test 2650 was attributable to the dislodging of the metal disk.....	31
Figure 33. Four layers of piezoelectric elements with various electric configurations were bonded to the target as shown on the left.....	32
Figure 34. Pre and post-test 2652 pictures of the QuickPack and PowerAct sensors.	33
Figure 35. Results from the eddy current gauge.....	34
Figure 36. Output from PA1.....	34
Figure 37. Output from QP1.....	35
Figure 38. Output from PA2.....	35
Figure 39. Output from QP2.....	36
Figure 40. Displacement of the center node in response to the ballistic event.....	37
Figure 41. Displacement of the center node in response to the ballistic event when a structural interference wave is generated by the piezoelectric elements in response to a high voltage pulse.	37

List of Tables

Table 1. Material properties of the armor system.....	5
Table 2. Test sequence and failure mechanisms for a ballistic test conducted at ARL.....	29
Table 3. Description of the integrated piezo tests.....	32
Table 4. Details of the four encapsulated piezoelectric wafers bonded to the Kevlar plate.....	33

Acknowledgments

Midé would like to acknowledge the following ARL personnel for their contribution to this work:

1. Mr. Tyrone Jones for the initiating the program and having the foresight to evaluate the use piezoelectric “smart” materials for shock mitigation during a ballistic event. Mr. Jones provided Midé with armor mechanic background and experimental ballistic tests results.
2. Mr. William Gooch for overall program support.
3. Mr. Neil Gniazdowski for setup and use of measuring and recording equipment.
4. Mr. Matt Burkins for setup and use of the ballistic laboratory and conducting tests.

Executive Summary

Midé Technology Corporation was approached by the U.S. Army Research Laboratory (ARL) to investigate the effect of using the unique effects of piezoelectric materials in order to reduce the magnitude of the ballistic shock of ballistic events. The program was set up to develop a three-dimensional (3-D) structural analysis code to simulate the effect of the piezo materials on the displacement of a Kevlar¹ 29 laminate armor plate. These models were to be calibrated via simple ballistic tests. Once the code was calibrated, an optimization and design effort would be completed in order to perform proof-of-concept tests.

Upon receiving the orthotropic material properties of the Kevlar 29 composite, Midé's research and development, which specializes in smart materials, decided to use a MATLAB²-based finite element approach that accurately models the 3-D anisotropic behavior of the armor. The model also included the ability to model piezoelectric material and its interaction with the Kevlar material.

Some delays in the process forced the testing to be postponed until very late in the program. This reduced the amount of time available for the calibration and optimization of the model. As an alternative, Midé agreed to integrate some of its off-the-shelf packaged piezoelectric actuators with Kevlar composite targets in order to test the effects of the ballistic events on the materials. This step was scheduled for the Phase I Option, and so certain tasks from Phase I moved into the option and vice versa.

Further difficulties in obtaining reliable data from the ballistic tests hindered calibration of the model. At this stage it was decided to simulate the tests that were conducted in ANSYS³, a commercial finite element analysis package. Correlation between the model and high speed video data, as well as data from the piezoelectric tests, was obtained as far as possible. The model was then used to investigate the effect of creating a destructive surface wave on reducing the maximum displacement of the impact point. Early, un-calibrated and un-optimized results indicate that a 27% reduction in the displacement of the impact point is possible when a high voltage pulse is delivered to a certain arrangement of piezoelectric materials.

These results are encouraging but should be validated by testing. Calibration of the model is scheduled early in the option. The model is ready to be optimized as soon as the calibration parameters are updated. This optimization will assist in a rapid design cycle to ensure that testing of an integrated system will still be performed during the option.

¹Kevlar is a registered trademark of E. I. DuPont de Nemours & Co., Inc.

²MATLAB is a registered trademark of The MathWorks.

³ANSYS, which is not an acronym, is a registered trademark of ANSYS, Inc.

The following is a summary of the achievements under each of the tasks as outlined in the work breakdown structure of the Phase I proposal.

Task 1: Develop and Understand Requirements

Midé had a productive “kick-off” meeting with the technical monitor at Aberdeen Proving Ground (APG). The meeting restated the objectives of the program, and the schedule and plan for the coming months were agreed upon. The technical monitor also provided Midé with literature and defined test parameters. Midé further received detailed specifications for the Kevlar plate to be used during the program.

Task 2: Parametric Modeling

A 3-D finite element model was constructed to study the anisotropic behavior of the armor material. This code was verified with previously published results and was used to understand the behavior of the armor system.

Task 3: Absorber Optimization

This task involved the integration of piezoelectric materials into the model. The voltage output and visual displacement correlations from the integrated model were validated with the limited experimental data available. Actuation control techniques, piezoelectric material size and placement, piezoelectric shunting techniques and other shock mitigation schemes need to be explored in a post-Phase I option.

Task 4: Preliminary Experiments

Ballistic experiments using polypropylene bullets shot at Kevlar targets at 1000 m/s were performed at APG. These tests include shots at targets with piezoelectric materials integrated into them. Some useful data were obtained during the tests, and more tests are scheduled in the period between the end of Phase I and the start of the option.

Task 5: Shock Absorber Design

A piezoelectric material configuration, size and actuation scheme was chosen to investigate the effect of producing a destructive surface wave in the Kevlar to reduce the displacement of the impact point. The result of this modeling effort was a 27% reduction in the translation of the impact point. This result is encouraging, but it must be noted that the model is not calibrated and that the result can only be verified with experiments in a post-Phase I option.

1. Description of Work Completed During Phase I

This section reports about the progress that was made under each of the proposed tasks. The original tasks are listed in the beginning of each chapter in *italics*.

1.1 Task 1: Develop and Understand Requirements

In this task, Midé worked with the U.S. Army Research Laboratory (ARL) to define a set of shock absorber requirements. ARL's experience and understanding of the dynamics of a ballistic impact were used to develop these requirements and to transfer knowledge to Midé personnel.

1.1.1 Kick-off Meeting

Midé had a productive meeting with the technical point of contact (TPOC) at Aberdeen Proving Ground (APG), Maryland. The meeting focused on the scheduling of tasks and the definition of the problem.

1.1.1.1 Problem Definition

Current bulletproof vest systems include a ceramic plate with a woven Kevlar 29 backing. The ceramic plate breaks up the bullet and reduces it to small pieces. The Kevlar backing then catches these pieces of ceramic and bullet, thus preventing them from penetrating the skin of the Soldier.

Midé gained a better understanding of the mechanics of the ballistic protection system. A main concern for personnel protection is the amount of displacement at the back of the armor system after a ballistic event. This displacement can cause damage to organs if not contained, often resulting in incapacitation the Soldier.

This displacement is a direct result from arresting the mass of target and penetrator that travels through the armor system after a ballistic event. The main focus of this project was to reduce the amount of displacement at the back of the armor protection system. Midé realized that the ballistic event has two components that need to be addressed.

First, the energy of the shock wave needs to be dissipated. Piezoceramics have been successfully applied to a number of high frequency-damping problems. Part of the program focused on how to effectively employ these ceramics so that maximum energy dissipation and damping can occur.

The second component is the momentum translation from the high speed, lightweight bullet to the slowly moving, higher mass armor vest. Ideally, the armor system translates all the momentum into a very slow moving mass that contacts a wide area of the body, thereby reducing the pressure on the body and minimizing the displacement of the body tissue.

A successful armor protection system will deal effectively with both these components in order to reduce the damage to the body.

The TPOC also supplied Midé with information about previous ballistic tests with ceramic and composite targets, evaluation of different periodic cellular materials and blunt trauma effects after low-velocity ballistic impacts.

1.1.2 Test Setup for Preliminary Tests

The approach to Task 1 was as follows:

1. Non-perforating small arms ballistic experiments that focused on collecting shock wave and displacement data off the back face of the target were conducted. These preliminary tests confirm the non-perforating test velocity for the test projectile into the target. The data that were collected are as follow:
 - Back face displacement versus time for 0- to 150-kHz range.
 - Shock wave speed and possibly shock wave pressure.
 - Maximum back face displacement.
2. Another experimental setup used was the composite panel attached to a steel plate and measured the force transmitted during the projectile impact with a load cell. Here would be an example of a worst case scenario of the force transmitted to the panel because of the coupling of the steel plate.
3. The data were obtained with the following transducers:
 - A crush gauge (or piezo pin transducers) with signal conditioning was initially used to get an initial measurement of the maximum back face displacement off the back of the target.
 - An eddy current gauge was set up at the back of the panel to give a displacement versus time reading and works for the 0- to 150-kHz frequency range. Velocity was obtained through post-processing differentiation.
 - A polyvinylidene fluoride transducer was used to measure the shock wave speed from the front face to the back face of the target and the shock wave pressure.
4. The data acquisition system was four, four-channel digital oscilloscopes.

1.1.3 Preliminary Test Definitions

The properties of the materials that were used in the preliminary tests and some of the test parameters are listed in table 1.

Table 1. Material properties of the armor system.

Parameters		
Target - Kevlar	Units	Value
Volume	cm ³	331.84
Size (L , W, t)	cm mm	L=W=22.86 t=6.35
Material Density	g/cm ³	1.44
Poisson's Ratio (in-plane)	--	0.12
Poisson's Ratio (out-of-plane)	--	0.4
Material Stiffness - x and y directions	GPa	24.1
Material Stiffness - z direction	GPa	10.4
Fiber Shear Strength	GPa	0.24
Matrix (Delamination Shear) Strength	MPa	48
Material Compression Strength	GPa	0.35
Thru Thickness Crush Strength	MPa	69
Penetrator – Polypropylene Plastic	Right cylinder projectile	
	Units	Value
Diameter	mm	12.57
Length	g	14.78
Weight	g	1.56
Density	g/cm ³	0.91
Velocity (at impact)	m/s	300-up
Tensile strength at yield	MPa	35.85
Tensile elongation at break	%	600
Tensile modulus	GPa	1.65
Flexural modulus	GPa	1.59
Flexural strength	MPa	48.26
Notched izod impact strength	J/m	60

1.2 Task 2: Parametric Modeling

In this task, Midé worked with ARL to develop a parametric model with which the performance of a shock absorber design was evaluated and validated.

Upon receiving the orthotropic material properties of the Kevlar, Midé decided to use a MATLAB⁴-based finite element approach that accurately models the 3-D anisotropic behavior of the armor. The code is attached as appendix A. This code was verified as far as possible and it was used to understand the dynamics of the impact and the resultant stresses that a piezo mitigation system must address. Figure 1 shows the model and figures 2 through 4 are the first three flexible modes predicted by the model. Results of an impact simulation are in figures 5 through 7 and time responses in figures 8 and 9.

⁴MATLAB is a registered trademark of The MathWorks.

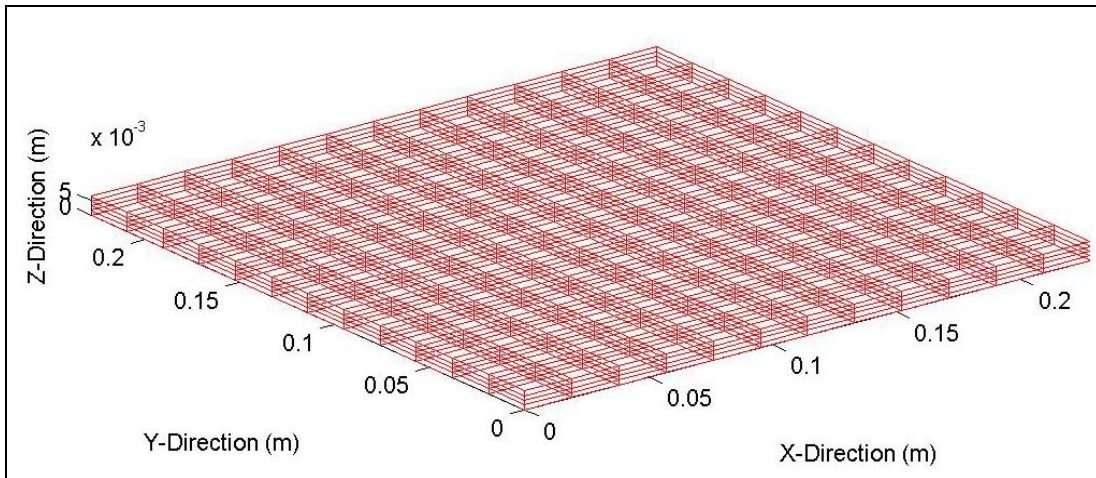


Figure 1. Finite element model.

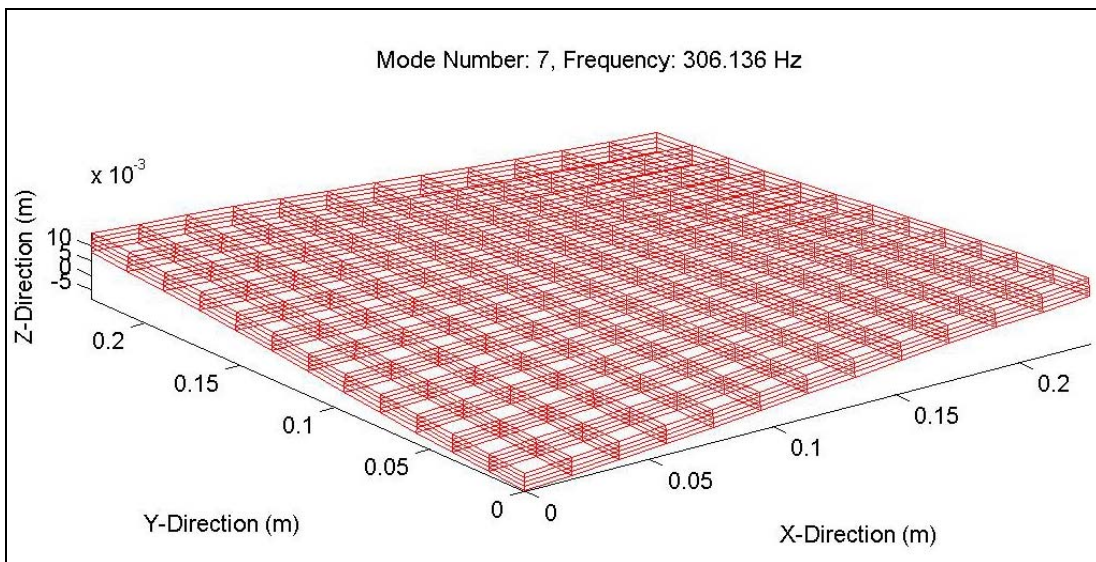


Figure 2. First non-rigid resonant mode shape.

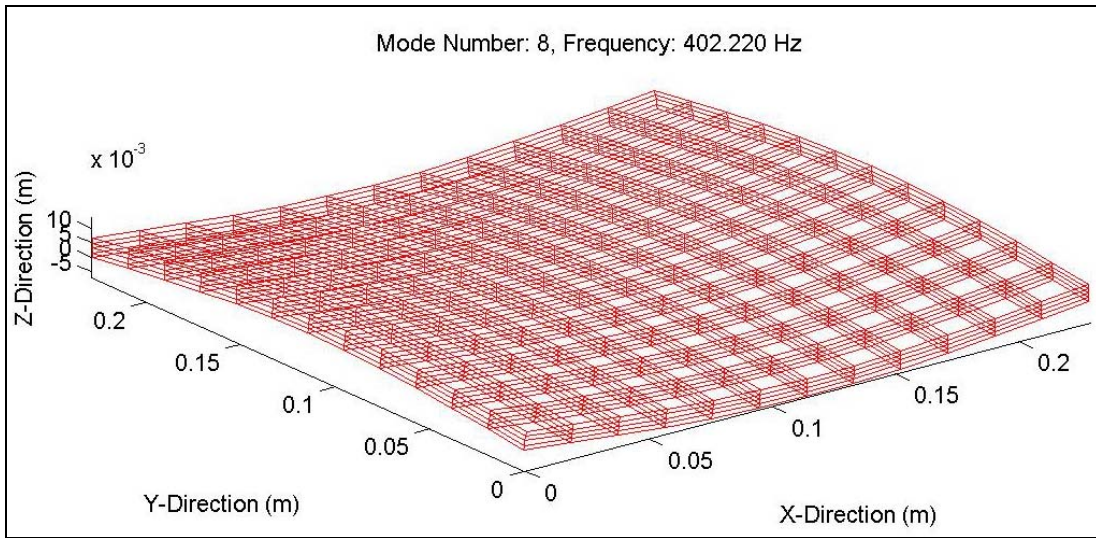


Figure 3. Second non-rigid resonant mode shape.

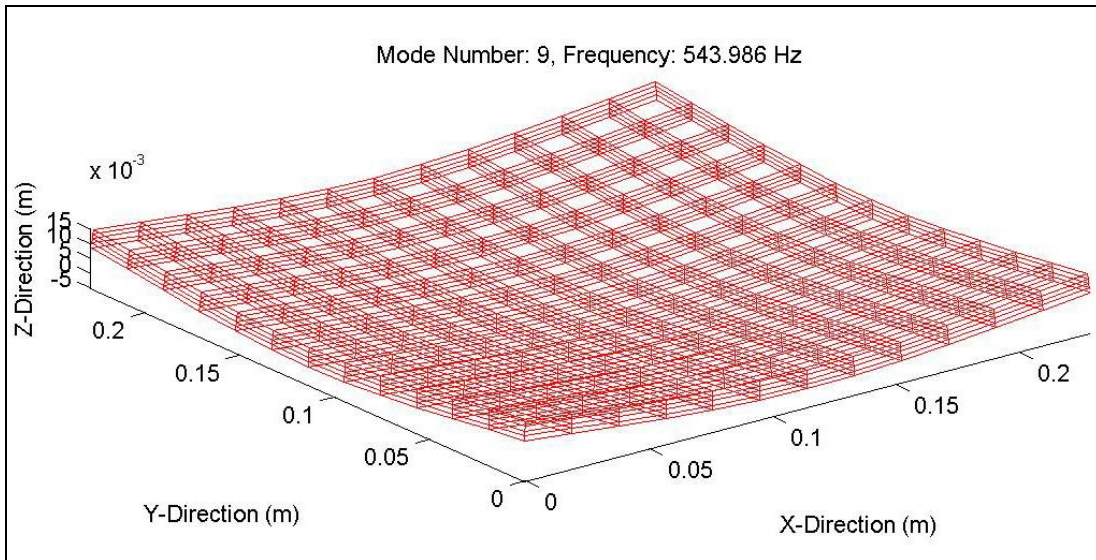


Figure 4. Third non-rigid resonant mode shape.

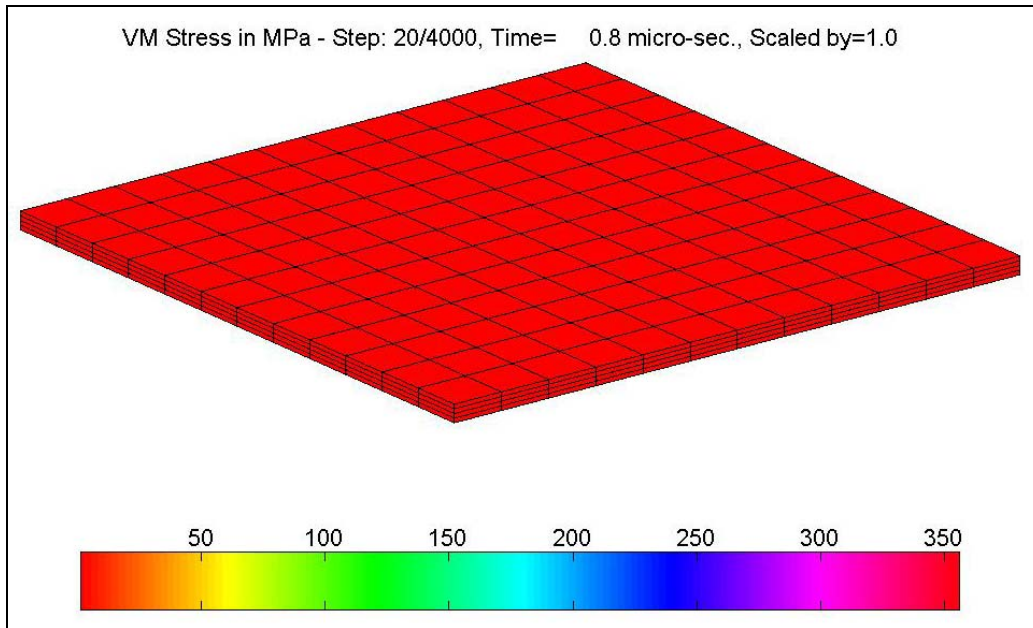


Figure 5. Von Mises stress at 0.8 μ s after the 1.56-gram projectile impacted the center of the plate at 450 m/s. (Note that the top surface is not deformed yet and that the damage is limited to the impact point.)

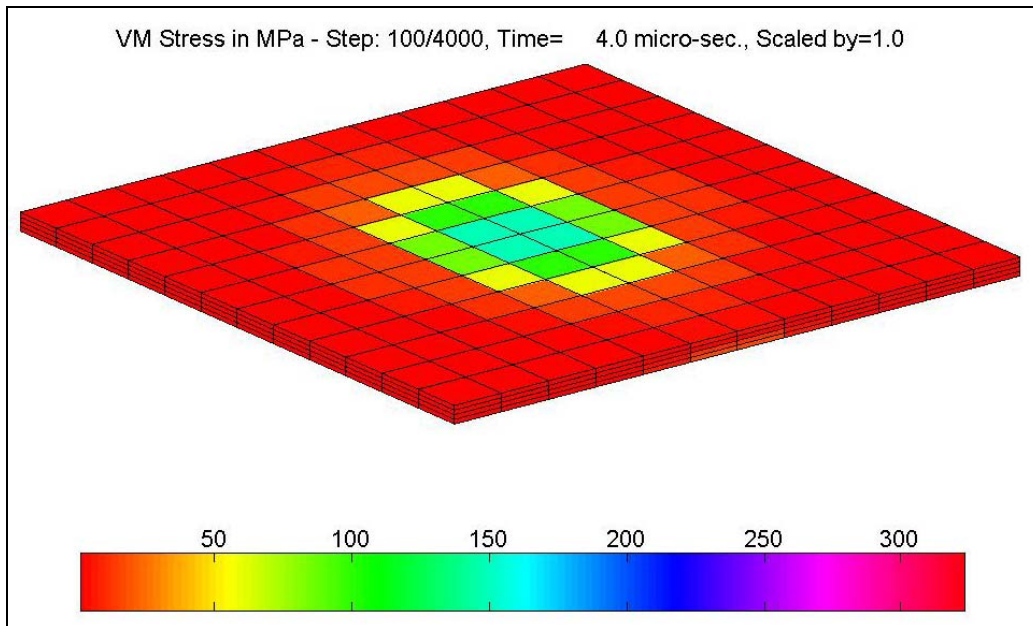


Figure 6. Von Mises stress at 4 μ s after the 1.56-gram projectile impacted the center of the plate at 450 m/s. (The stress on the top surface has increased but little or no deformation is visible. The maximum top surface Von Mises Stress is around 155 MPa.)

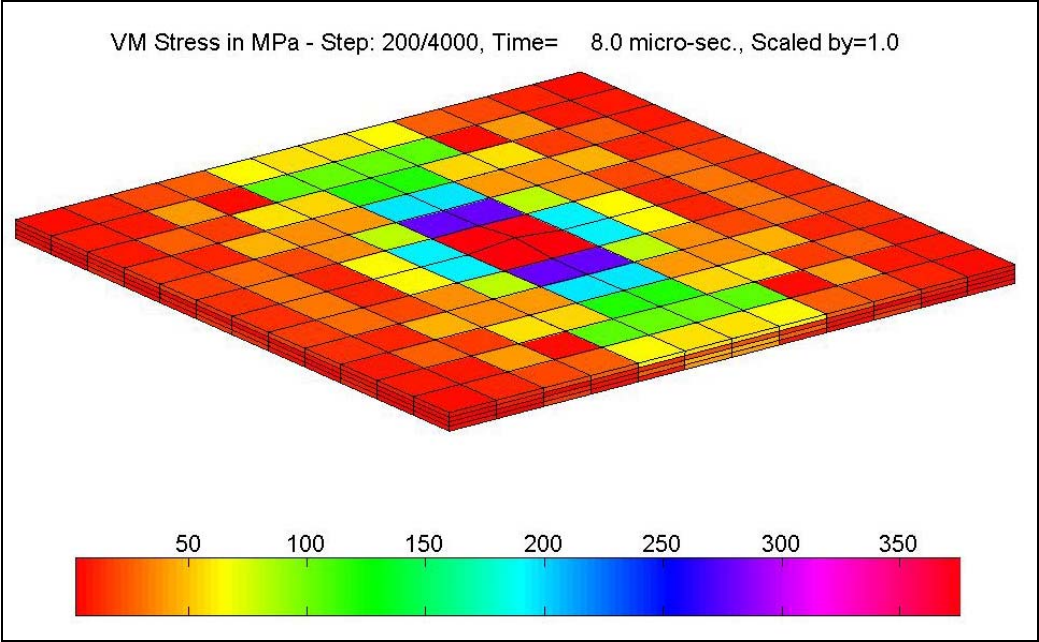


Figure 7. Von Mises stress at 8 μ s after the 1.56-gram projectile impacted the center of the plate at 450 m/s. (Clear deformation is visible at this point with the top surface near 350 MPa.)

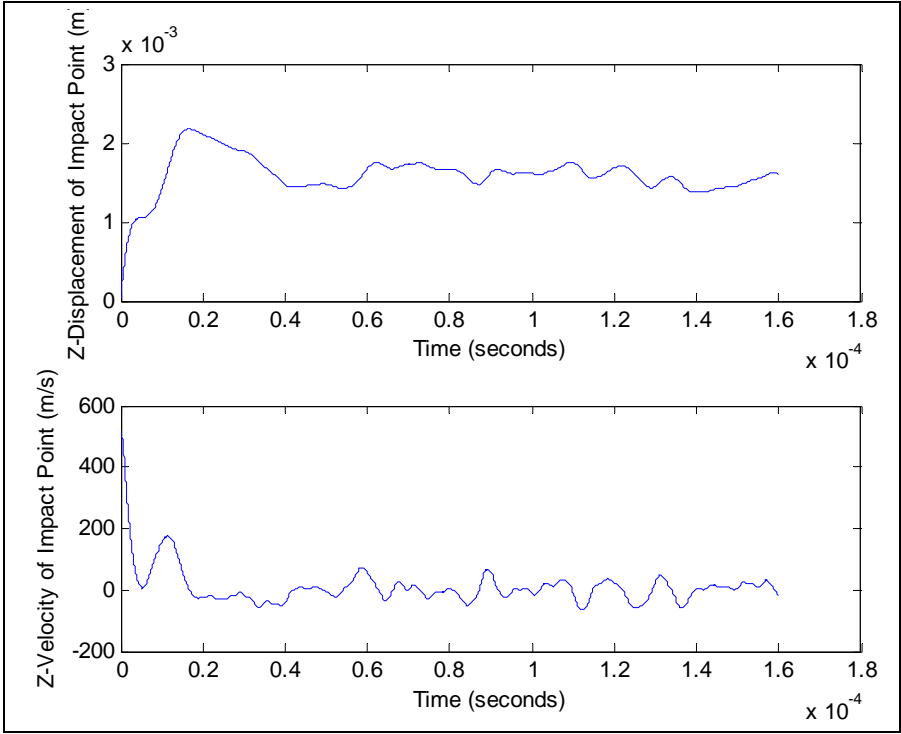


Figure 8. Displacement and velocity (deformation) of impact point.

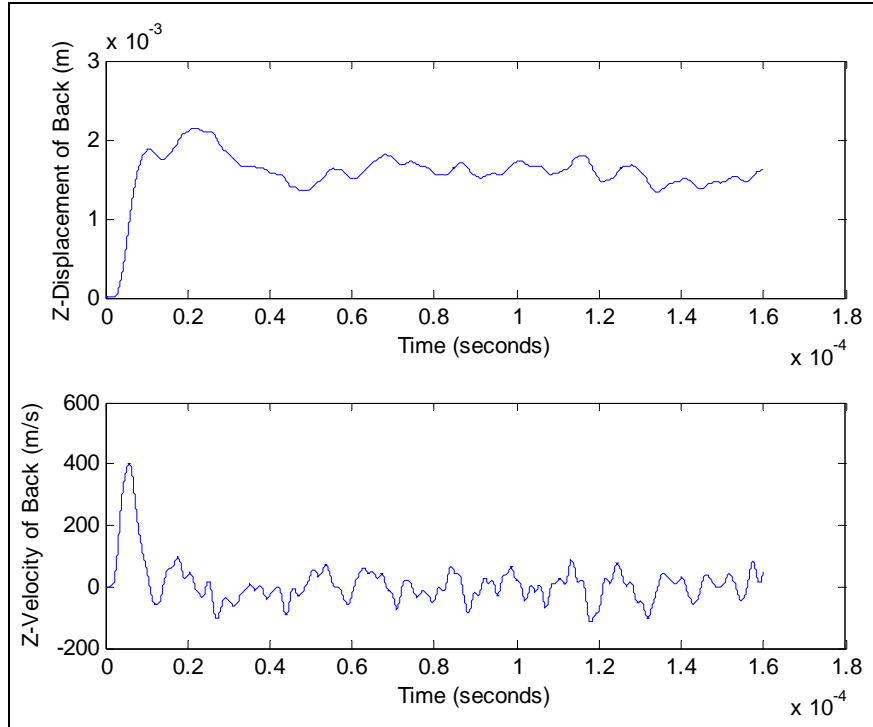


Figure 9. Displacement and velocity (deformation) of top surface directly above the impact point.

1.3 Task 3: Absorber Optimization

The models of Task 2 were used to establish a design, to optimize the design, and to estimate the performance of the design.

1.3.1 Finite Element Model Formulation

Midé uses the National Center for Supercomputing Applications structural analysis system Nastran⁵, which is a finite element analysis program. Nastran does not have a piezoelectric element in its library. Initially, the cost of ANSYS which does have a piezoelectric element was considered prohibitive, so Midé decided to evaluate the performance of different geometries of active (piezo) and passive materials, with its MATLAB-based finite element code. It is easier to generate many models in MATLAB compared to the alternative of using Nastran to generate the finite element models and then importing the finite element models into MATLAB where the active elements can be modeled.

The Midé MATLAB finite element code is based on the hybrid stress finite element that has excellent accuracy even if the elements are distorted. This sub-section provides a quick review of the formulation of hybrid stress finite elements.

⁵Nastran is a trademark of the National Center for Supercomputing Applications.

In the hybrid finite element model, the strain-stress relationship is

$$\varepsilon = S\sigma \quad (1)$$

The stress is expressed in terms of the undetermined stress parameters β :

$$\sigma = P\beta \quad (2)$$

From the strain-displacement (q) relations,

$$\varepsilon = Bq \quad (3)$$

The Hellinger-Reissner functional (Π_R)

$$\Pi_R = \int_V \left[-B(\sigma_{ij}) + \sigma_{ij}\varepsilon_{ij} \right] dV - \int_{S_i} u_i T_i dS \quad (4)$$

with

$$\Pi_R = -\frac{1}{2} \beta^T \mathbf{H} \beta + \beta^T \mathbf{G} q - (Bq)^T \mathbf{Q} \quad (5)$$

where \mathbf{Q} are the external forces and where

$$\mathbf{H} = \int_V P^T S P dV \quad (6)$$

$$\mathbf{G} = \int_V B^T P dV \quad (7)$$

The operations $\partial \Pi_R / \partial \beta_r = 0$ yield

$$\beta = \mathbf{H}^{-1} \mathbf{G} \alpha \quad (8)$$

Eliminating β and substituting

$$\alpha = B^{-1} q \quad (9)$$

we obtain

$$\mathbf{k} q = \mathbf{Q} \quad (10)$$

where the stiffness matrix is given by

$$H_{18 \times 18} = \left[P_{18 \times 6}^T S_{6 \times 6} P_{6 \times 18} \right] W_{Intg} \quad (11)$$

$$\mathbf{k} = G_{24 \times 18}^T H_{18 \times 18}^{-1} G_{18 \times 24} = \frac{B_{24 \times 6}^T P_{6 \times 18}}{|J|} \left[P_{18 \times 6}^T S_{6 \times 6} P_{6 \times 18} \right]^{-1} \frac{P_{18 \times 6}^T B_{6 \times 24}}{|J|} W_{Intg}$$

where

$$G_{18 \times 24} = \int_V B^T P dV = \frac{P_{18 \times 6}^T B_{6 \times 24}}{|J|} W_{Intg} \quad (12)$$

1.3.2 Anisotropic Materials

The first modification of the existing MATLAB code was to include in the model the ability to use anisotropic materials. Given the Jacobian of an element,

$$\begin{Bmatrix} \frac{\partial}{\partial \xi} \\ \frac{\partial}{\partial \eta} \\ \frac{\partial}{\partial \zeta} \end{Bmatrix} = \begin{bmatrix} \frac{\partial x}{\partial \xi} & \frac{\partial y}{\partial \xi} & \frac{\partial z}{\partial \xi} \\ \frac{\partial x}{\partial \eta} & \frac{\partial y}{\partial \eta} & \frac{\partial z}{\partial \eta} \\ \frac{\partial x}{\partial \zeta} & \frac{\partial y}{\partial \zeta} & \frac{\partial z}{\partial \zeta} \end{bmatrix} \begin{Bmatrix} \frac{\partial}{\partial x} \\ \frac{\partial}{\partial y} \\ \frac{\partial}{\partial z} \end{Bmatrix} = \mathbf{J} \begin{Bmatrix} \frac{\partial}{\partial x} \\ \frac{\partial}{\partial y} \\ \frac{\partial}{\partial z} \end{Bmatrix} \quad (13)$$

The orientation of element in the global coordinate system, given its nodal connectivity numbering, can be determined as the normalized inverse of the Jacobian:

$$\mathbf{T} = \frac{\mathbf{J}^{-1}}{|\mathbf{J}^{-1}|} \quad (14)$$

Given the definition of the compliance matrix \mathbf{S} ,

$$\begin{Bmatrix} \varepsilon_x \\ \varepsilon_y \\ \varepsilon_z \\ \gamma_{yz} \\ \gamma_{zx} \\ \gamma_{xy} \end{Bmatrix} = \begin{bmatrix} \frac{1}{E_{xx}} & -\frac{\nu_{yx}}{E_{yy}} & -\frac{\nu_{zx}}{E_{zz}} & 0 & 0 & 0 \\ -\frac{\nu_{xy}}{E_{xx}} & \frac{1}{E_{yy}} & -\frac{\nu_{zy}}{E_{zz}} & 0 & 0 & 0 \\ -\frac{\nu_{xz}}{E_{xx}} & -\frac{\nu_{yz}}{E_{yy}} & \frac{1}{E_{zz}} & 0 & 0 & 0 \\ 0 & 0 & 0 & \frac{2(1+\nu_{yz})}{E_{xx}} & 0 & 0 \\ 0 & 0 & 0 & 0 & \frac{2(1+\nu_{zx})}{E_{yy}} & 0 \\ 0 & 0 & 0 & 0 & 0 & \frac{2(1+\nu_{xy})}{E_{zz}} \end{bmatrix} \begin{Bmatrix} \sigma_x \\ \sigma_y \\ \sigma_z \\ \tau_{yz} \\ \tau_{zx} \\ \tau_{xy} \end{Bmatrix} = \mathbf{S} \begin{Bmatrix} \sigma_x \\ \sigma_y \\ \sigma_z \\ \tau_{yz} \\ \tau_{zx} \\ \tau_{xy} \end{Bmatrix} \quad (15)$$

The compliance matrix $\bar{\mathbf{S}}$ in the element coordinate system is

$$\bar{\mathbf{S}} = \begin{bmatrix} \mathbf{T}_{6 \times 6} & [0]_{6 \times 6} \\ [0]_{6 \times 6} & \mathbf{T}_{6 \times 6} \end{bmatrix}^T \begin{bmatrix} \frac{1}{E_{xx}} & -\frac{\nu_{yx}}{E_{yy}} & -\frac{\nu_{zx}}{E_{zz}} & 0 & 0 & 0 \\ -\frac{\nu_{xy}}{E_{xx}} & \frac{1}{E_{yy}} & -\frac{\nu_{zy}}{E_{zz}} & 0 & 0 & 0 \\ -\frac{\nu_{xz}}{E_{xx}} & -\frac{\nu_{yz}}{E_{yy}} & \frac{1}{E_{zz}} & 0 & 0 & 0 \\ 0 & 0 & 0 & \frac{2(1+\nu_{yz})}{E_{xx}} & 0 & 0 \\ 0 & 0 & 0 & 0 & \frac{2(1+\nu_{zx})}{E_{yy}} & 0 \\ 0 & 0 & 0 & 0 & 0 & \frac{2(1+\nu_{xy})}{E_{zz}} \end{bmatrix} \begin{bmatrix} \mathbf{T}_{6 \times 6} & [0]_{6 \times 6} \\ [0]_{6 \times 6} & \mathbf{T}_{6 \times 6} \end{bmatrix} \quad (16)$$

1.3.3 Modeling of Piezoelectric Materials

The next step in expanding the capabilities of the MATLAB code was to determine the voltage generated by the piezo elements when deformed and the deformation they induce when a voltage is applied. A piezoelectric material is transversely isotropic. In the Institute of Electrical and Electronics Engineers Standard (STD-176-1978), the relationship among dielectric displacement (D), mechanical stress (T), the electric field (E) and mechanical strain is (S)

$$\begin{Bmatrix} D_1 \\ D_2 \\ D_3 \\ S_1 \\ S_2 \\ S_3 \\ S_4 \\ S_5 \\ S_6 \end{Bmatrix} = \begin{bmatrix} \tilde{\varepsilon}_{11}^T & 0 & 0 & 0 & 0 & 0 & 0 & d_{15} & 0 \\ 0 & \tilde{\varepsilon}_{22}^T & 0 & 0 & 0 & 0 & d_{15} & 0 & 0 \\ 0 & 0 & \tilde{\varepsilon}_{33}^T & d_{31} & d_{31} & d_{33} & 0 & 0 & 0 \\ 0 & 0 & d_{31} & s_{11}^E & s_{12}^E & s_{13}^E & 0 & 0 & 0 \\ 0 & 0 & d_{31} & s_{12}^E & s_{22}^E & s_{23}^E & 0 & 0 & 0 \\ 0 & 0 & d_{33} & s_{13}^E & s_{23}^E & s_{33}^E & 0 & 0 & 0 \\ 0 & d_{15} & 0 & 0 & 0 & 0 & s_{44}^E & 0 & 0 \\ d_{15} & 0 & 0 & 0 & 0 & 0 & 0 & s_{55}^E & 0 \\ 0 & 0 & 0 & 0 & 0 & 0 & 0 & 0 & s_{66}^E \end{bmatrix} \begin{Bmatrix} E_1 \\ E_2 \\ E_3 \\ T_1 \\ T_2 \\ T_3 \\ T_4 \\ T_5 \\ T_6 \end{Bmatrix} \quad (17)$$

where ε is the permittivity of the material and it is assumed to be isothermal. In engineering notation,

$$\begin{Bmatrix} \lambda_1 \\ \lambda_2 \\ \lambda_3 \\ \varepsilon_1 \\ \varepsilon_2 \\ \varepsilon_3 \\ \varepsilon_4 \\ \varepsilon_5 \\ \varepsilon_6 \end{Bmatrix} = \begin{bmatrix} \tilde{\varepsilon}_{11}^T & 0 & 0 & 0 & 0 & 0 & 0 & d_{15} & 0 \\ 0 & \tilde{\varepsilon}_{22}^T & 0 & 0 & 0 & 0 & d_{15} & 0 & 0 \\ 0 & 0 & \tilde{\varepsilon}_{33}^T & d_{31} & d_{31} & d_{33} & 0 & 0 & 0 \\ 0 & 0 & d_{31} & s_{11}^E & s_{12}^E & s_{13}^E & 0 & 0 & 0 \\ 0 & 0 & d_{31} & s_{12}^E & s_{22}^E & s_{23}^E & 0 & 0 & 0 \\ 0 & 0 & d_{33} & s_{13}^E & s_{23}^E & s_{33}^E & 0 & 0 & 0 \\ 0 & d_{15} & 0 & 0 & 0 & 0 & s_{44}^E & 0 & 0 \\ d_{15} & 0 & 0 & 0 & 0 & 0 & 0 & s_{55}^E & 0 \\ 0 & 0 & 0 & 0 & 0 & 0 & 0 & 0 & s_{66}^E \end{bmatrix} \begin{Bmatrix} E_1 \\ E_2 \\ E_3 \\ \sigma_1 \\ \sigma_2 \\ \sigma_3 \\ \sigma_4 \\ \sigma_5 \\ \sigma_6 \end{Bmatrix} \quad (18)$$

This can be re-written in block matrix form as

$$\begin{Bmatrix} \lambda \\ \varepsilon \end{Bmatrix} = \begin{bmatrix} \tilde{\varepsilon} & e \\ e^T & S^E \end{bmatrix}_{9 \times 9} \begin{Bmatrix} E \\ \sigma \end{Bmatrix} \quad (19)$$

where the coupling coefficient is now e and c represents stiffness.

$$\begin{Bmatrix} \lambda_1 \\ \lambda_2 \\ \lambda_3 \end{Bmatrix} = \begin{bmatrix} \tilde{\varepsilon}_{11} & 0 & 0 \\ 0 & \tilde{\varepsilon}_{22} & 0 \\ 0 & 0 & \tilde{\varepsilon}_{33} \end{bmatrix} \begin{Bmatrix} E_1 \\ E_2 \\ E_3 \end{Bmatrix} + \begin{bmatrix} 0 & 0 & 0 & 0 & d_{15} & 0 \\ 0 & 0 & 0 & d_{15} & 0 & 0 \\ d_{31} & d_{31} & d_{33} & 0 & 0 & 0 \end{bmatrix} \begin{Bmatrix} \sigma_1 \\ \sigma_2 \\ \sigma_3 \\ \sigma_4 \\ \sigma_5 \\ \sigma_6 \end{Bmatrix} \quad (20)$$

$$\{\lambda\} = [\tilde{\varepsilon}] \{E\} + [e] \{\sigma\}$$

$$\begin{Bmatrix} \varepsilon_1 \\ \varepsilon_2 \\ \varepsilon_3 \\ \varepsilon_4 \\ \varepsilon_5 \\ \varepsilon_6 \end{Bmatrix} = [e]^T \{E\} + \begin{bmatrix} S_{11}^E & S_{13}^E & S_{13}^E & 0 & 0 & 0 \\ S_{12}^E & S_{22}^E & S_{23}^E & 0 & 0 & 0 \\ S_{13}^E & S_{23}^E & S_{33}^E & 0 & 0 & 0 \\ 0 & 0 & 0 & S_{44}^E & 0 & 0 \\ 0 & 0 & 0 & 0 & S_{55}^E & 0 \\ 0 & 0 & 0 & 0 & 0 & S_{66}^E \end{bmatrix} \begin{Bmatrix} \sigma_1 \\ \sigma_2 \\ \sigma_3 \\ \sigma_4 \\ \sigma_5 \\ \sigma_6 \end{Bmatrix} \quad (21)$$

$$\{\varepsilon\} = [e]^T \{E\} + [S^E] \{\sigma\}$$

The piezo can be a sensor ($\lambda = 0$), which yields the following equations:

$$\begin{aligned} \lambda = \tilde{\varepsilon}E + e\sigma = 0 &\Rightarrow E = -(\tilde{\varepsilon})^{-1} e\sigma \\ \varepsilon = e^T E + S^E \sigma = -e^T (\tilde{\varepsilon})^{-1} e\sigma + S^E \sigma \end{aligned} \quad (22)$$

or it can be driven by an applied electric field:

$$\begin{aligned} \lambda = \tilde{\varepsilon}E_{applied} + e\sigma \\ \varepsilon = e^T E_{applied} + S^E \sigma \end{aligned} \quad (23)$$

$e^T E_{applied}$ is a forcing term and can be included in the finite element model as n virtual work terms.

This was implemented in the MATLAB code.

Place this in the Hellinger-Reissner functional:

$$\begin{aligned} \Pi_R &= -\frac{1}{2} \beta^T \mathbf{H} \beta + \int_V \sigma_{ij} e^T E_{Applied} dV + \beta^T \mathbf{J} \alpha - (B\alpha)^T \mathbf{Q} \\ &= -\frac{1}{2} \beta^T \mathbf{H} \beta + \beta^T \mathbf{F} + \beta^T \mathbf{J} \alpha - (B\alpha)^T \mathbf{Q} \beta^T \end{aligned} \quad (24)$$

Where \mathbf{F}

$$\mathbf{F}E = \int_V P^T e^T dVE \quad (25)$$

This yields a new “forcing” term:

$$\begin{aligned} \mathbf{Q}_E &= \beta^T \mathbf{F}E = [B^{-1}]_{24 \times 6}^T [J^{-1}]_{6 \times 18}^T \mathbf{F}_{18 \times 3} E_{3 \times 1} \\ &= \beta^T \mathbf{F} \begin{bmatrix} \frac{1}{t_{xx}} & 0 & 0 \\ 0 & \frac{1}{t_{yy}} & 0 \\ 0 & 0 & \frac{1}{t_{zz}} \end{bmatrix} V_{3 \times 1} \\ &= \alpha^T \mathbf{G}^T [\mathbf{H}^{-1}]^T \mathbf{F} \begin{bmatrix} \frac{1}{t_{xx}} & 0 & 0 \\ 0 & \frac{1}{t_{yy}} & 0 \\ 0 & 0 & \frac{1}{t_{zz}} \end{bmatrix} V_{3 \times 1} \end{aligned} \quad (26)$$

The active strain is

$$\lambda = \tilde{\varepsilon}_{3x3} E_{3x1} + e_{3x6} \sigma_{6x1} \quad (27)$$

when there is an applied field and without an applied field, the generated field is

$$\begin{aligned} \lambda = \tilde{\varepsilon} E + e \sigma = 0 &\Rightarrow E = -(\tilde{\varepsilon})^{-1} e \sigma \\ \varepsilon = e^T E + S^E \sigma &= -e^T (\tilde{\varepsilon})^{-1} e \sigma + S^E \sigma \end{aligned} \quad (28)$$

Note that the same coordinate transformation needs to be performed if the material properties are aligned along the element coordinate system.

Figure 10 is a simple example where a voltage was placed over an element in the Z-direction (the d_{33} direction).

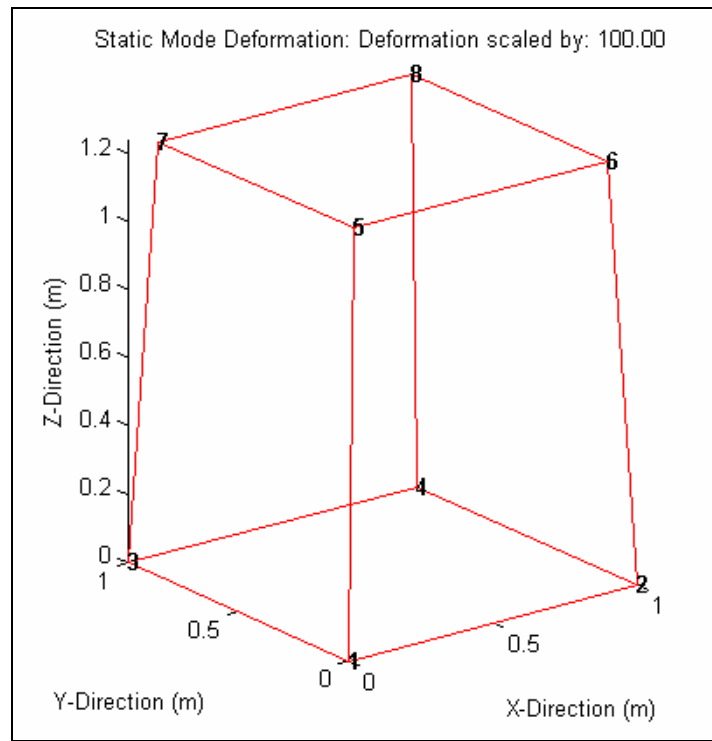


Figure 10. Deformation of a piezo cube when a voltage is applied across the d_{33} (Z-) direction. (The bottom corners are fixed and the cube expands in the Z-direction while contracting in the X- and Y-directions. The constraints introduce stresses in the cube.)

1.3.4 Linear Results

The finite elements were programmed in FORTRAN (Formula Translator) and linked with MATLAB executable files. The model was used to examine the performance of the ceramic–glass-reinforced plastic (GRP) composite targets of Straßburger, Senf, Burkins, and Gooch (1996). This section reports the results where the material behavior was assumed to be linear. The next step was to perform a nonlinear large deformation analysis where elements in which the stresses exceed

failure criteria are eliminated from the analysis. Figure 11 shows the linear first mode predicted by the Midé code. Note that for these results, clamped boundary conditions were assumed in the model. The total target mass is predicted to be 11.40 kg or 25.08 lb.

The model was also used to examine the behavior of the target if the boundary conditions were assumed to be simply supported.

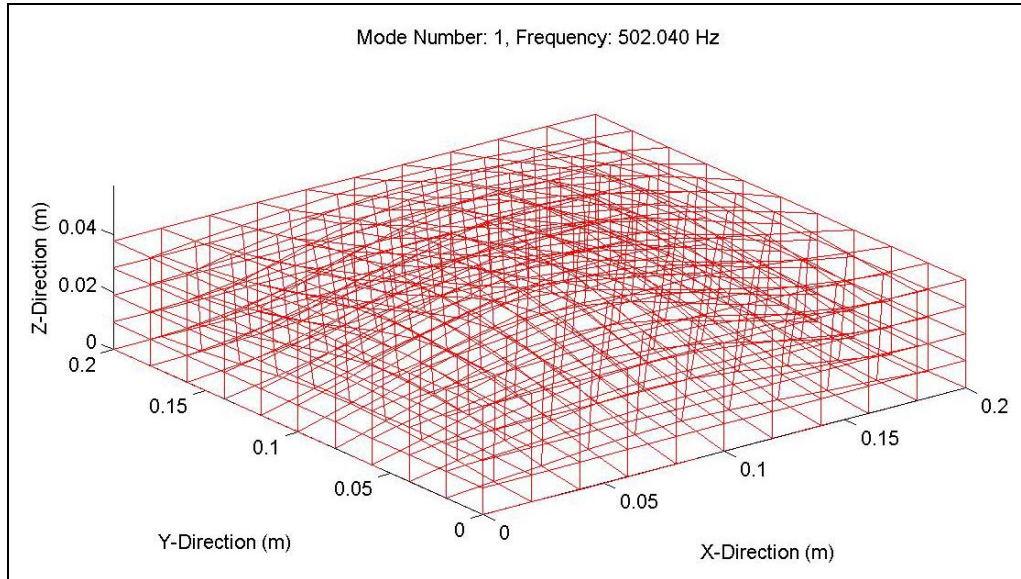


Figure 11. First mode shape of the ceramic-GRP composite target predicted by the Midé code. (Boundary conditions were clamped.)

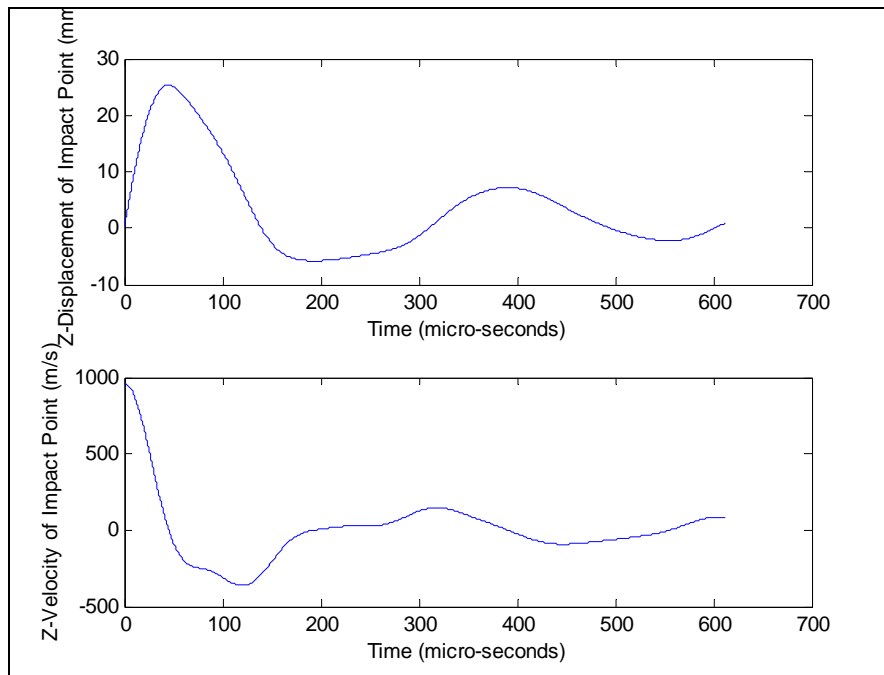


Figure 12. Displacement and velocity (deformation) of impact point. (Boundary conditions were clamped.)

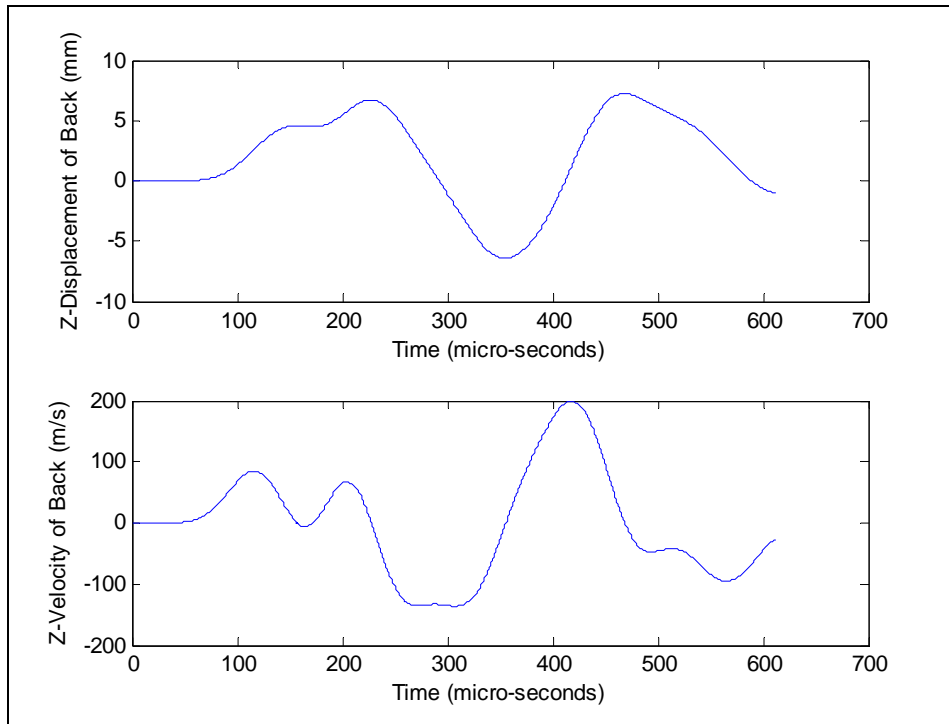


Figure 13. Displacement and velocity (deformation) of the top surface directly above the impact point. (Boundary conditions were clamped.)

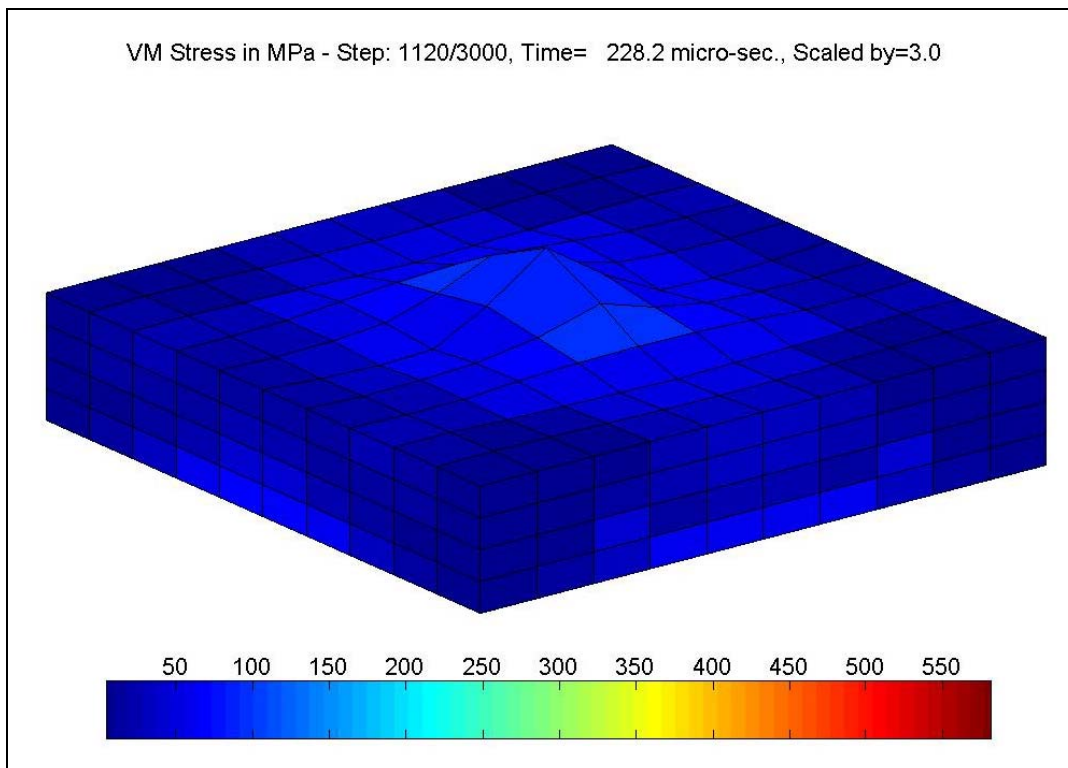


Figure 14. Predicted von Mises stresses at 230 microseconds (μ s) after impact. (Boundary conditions were clamped.)

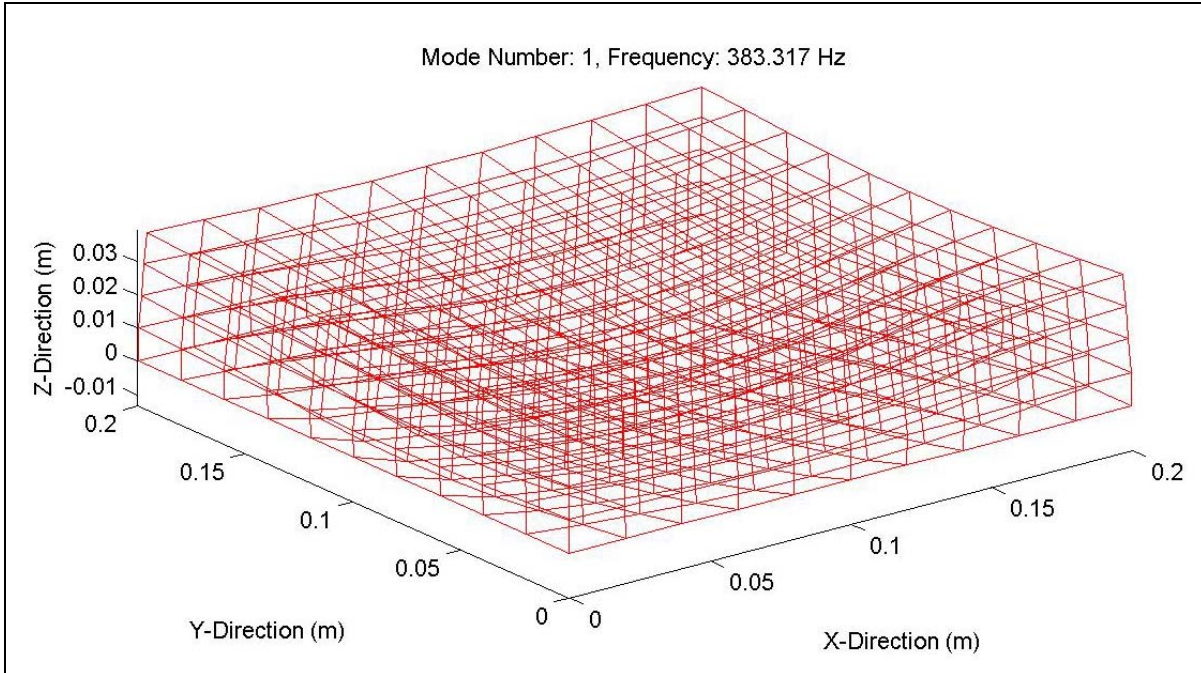


Figure 15. First mode shape of the ceramic-GRP composite target predicted by the Midé code. (Boundary conditions were simply supported.)

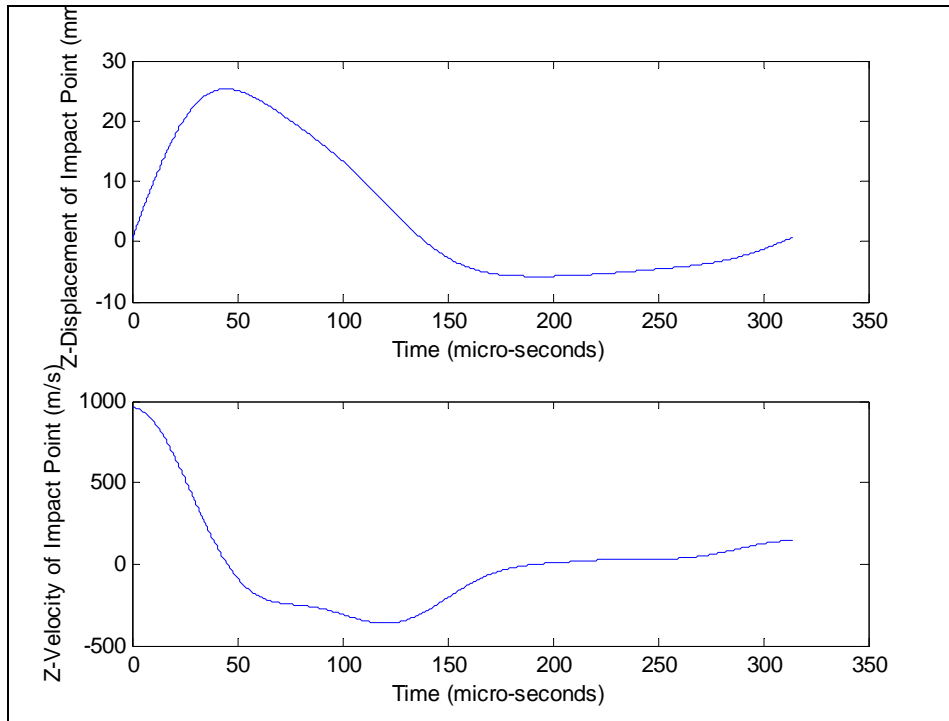


Figure 16. Displacement and velocity (deformation) of impact point. (Boundary conditions were simply supported.)

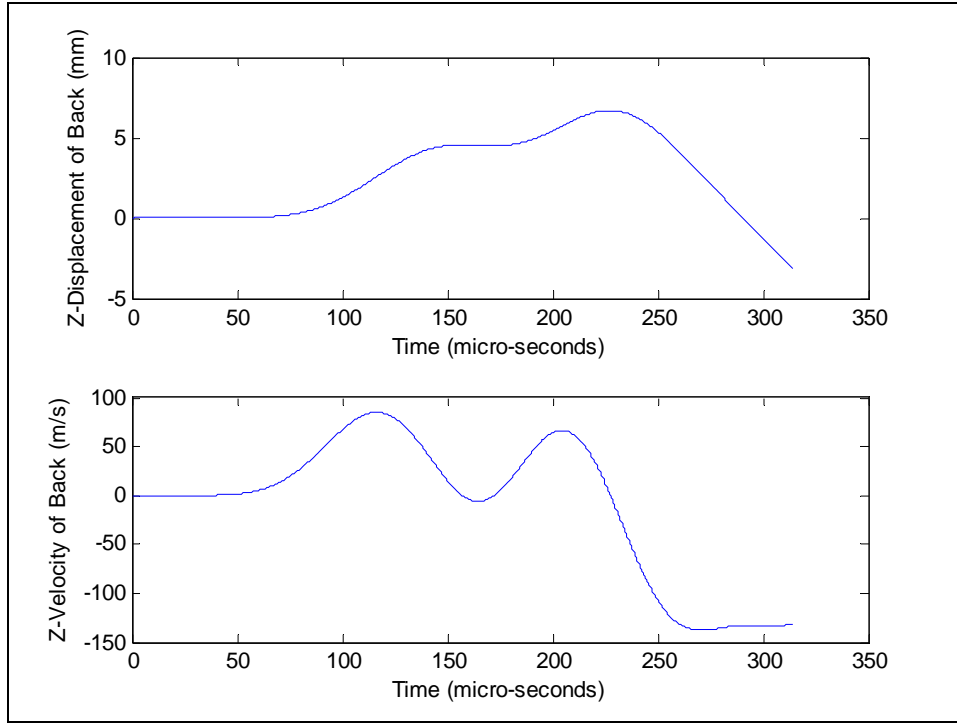


Figure 17. Displacement and velocity (deformation) of the top surface directly above the impact point. (Boundary conditions were simply supported.)

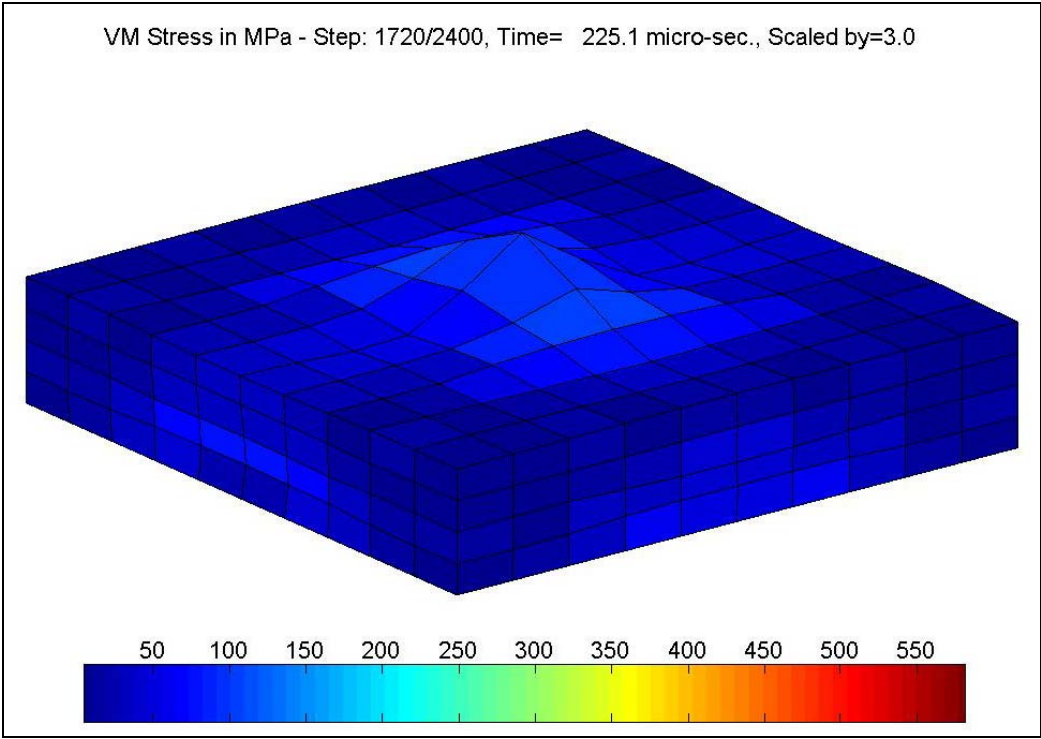


Figure 18. Predicted von Mises stresses at 230 micro-seconds after impact. (Boundary conditions were simply supported.)

As expected, the linear analysis was substantially different from the results reported in Straßburger et al. (1996). However Midé code can now predict the voltages generated by piezo-materials and is ready for studies of how the piezo-elements can be used to reduce the deformation of the back plate.

1.3.5 ANSYS Finite Element Model

Initially, Midé considered the cost of obtaining ANSYS specifically for this program to be prohibitive. Another Midé program had the funds available and decided to purchase the FEA package. This allowed Midé to generate an alternate finite element model for this program. The advantages of using ANSYS instead of the MATLAB model are as follow:

- A finer grid can be modeled.
- The actual models can be created in a solid modeling program and imported into the FEA package.
- Optimization is supported.
- Highly detailed piezoelectric models are available.
- Memory management schemes in ANSYS allow for more detailed analysis.
- Time history and animation plots are easily obtained.

It was thus decided at a late stage in the program to change to the ANSYS model.

1.3.5.1 ANSYS Model Description

Figure 19 illustrates the meshed ANSYS model. The model consists of tetrahedral elements for the Kevlar parts and solid bricks for the piezo parts. Figure 19 shows the model in a deformed state. The model's boundary conditions are placed at three nodes on every corner on the piezo side of the Kevlar plate in every direction. A simple assumption was to model the bullet impact as an initial velocity on the nodes surrounding the center of the plate with a 0.5-inch diameter. This velocity was set at 1000 m/s.

The piezo elements were constrained so that all the elements on their top and bottom (attached to the Kevlar) surfaces were electrically connected to each other. This had the same effect as placing an electrode over these surfaces and modeled the QuickPack⁶ and PowerAct sensors and actuators well.

A typical result of the analysis is shown in figure 20. Here, the elements are deformed and highlighted according to their displacement in the z direction (direction the bullet is traveling). The shock waves can clearly be seen on the surface, causing the displacements.

⁶QuickPack and PowerAct are trademarks of Midé Technology Corporation.

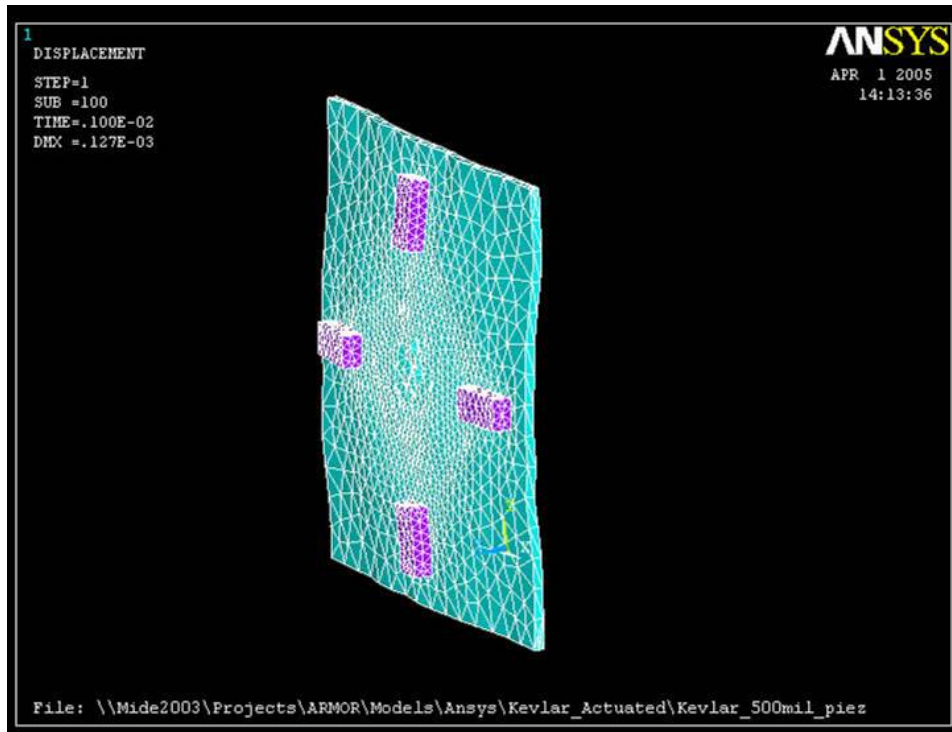


Figure 19. The meshed ANSYS model.

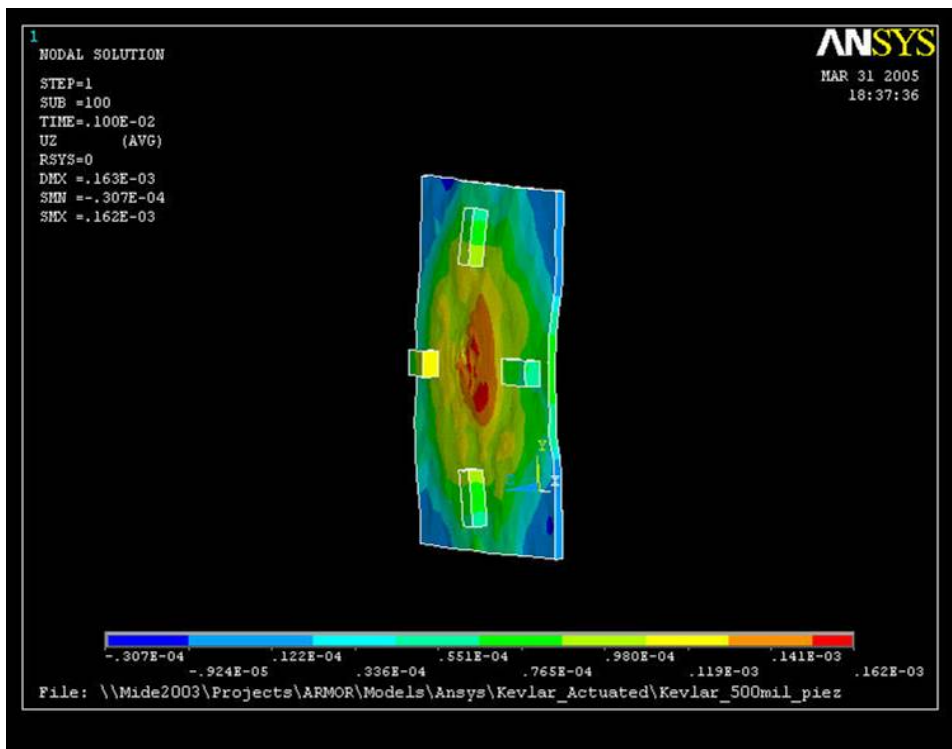


Figure 20. A typical result from the ANSYS analysis illustrating the nodal displacement in the z direction.

1.3.5.2 Time Step Displacement Comparisons

The following series of images compares the displacement output of the ANSYS model to that of the high speed video camera for test 2649. The high speed video camera has a shutter speed of $121 \mu\text{s}/\text{frame}$. The model was run with a $10\text{-}\mu\text{s}$ interval. Every 12th step of the output of the model is shown in table 2. The plate is c-clamped to the holder and struck on the face contacting the frame. The impact is below the black tape.

It is interesting to note how the model captures the initial ballistic event, causing the sharp bubble in the Kevlar, and the secondary wave that displaces the Kevlar from the frame. This comparison shows that the model is somewhat representative of reality. Unfortunately, real displacement data were not available and a true calibration of the model was not possible.

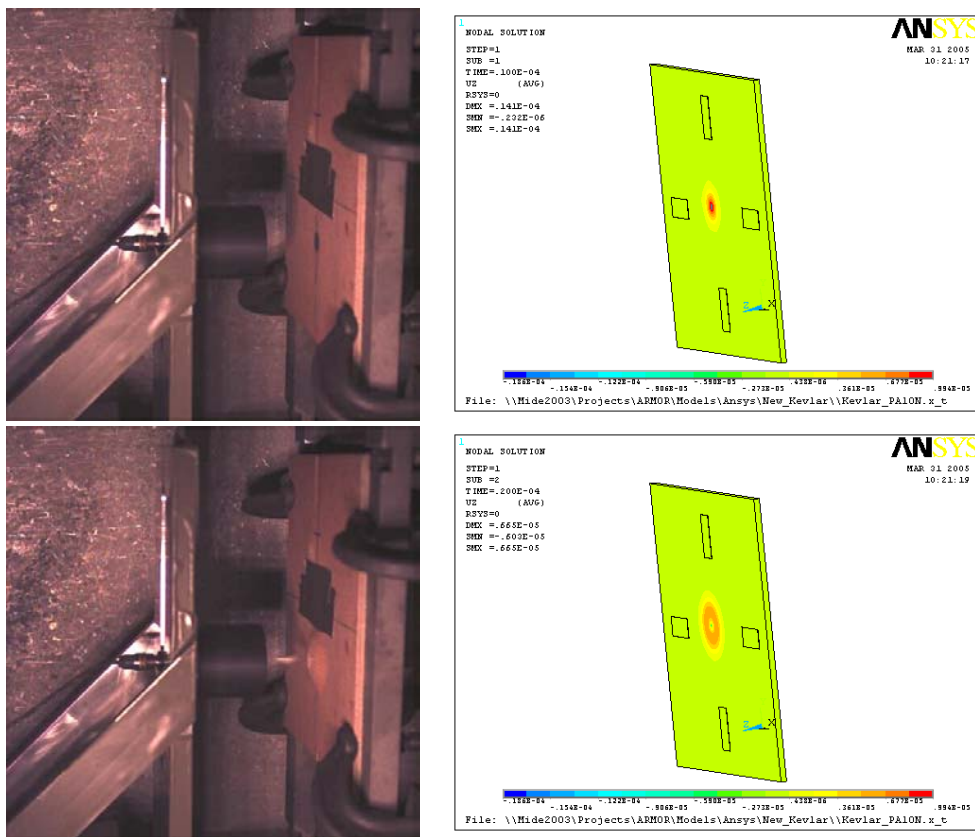


Figure 21. Comparison of high speed video and the ANSYS model.

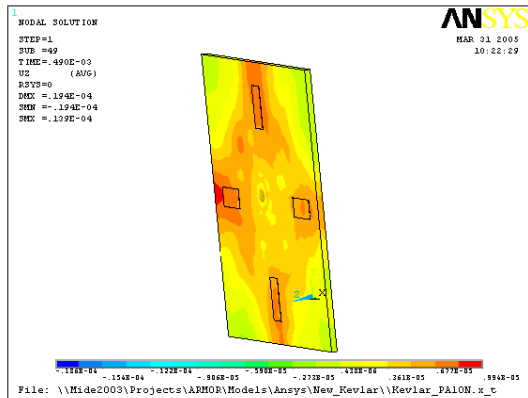
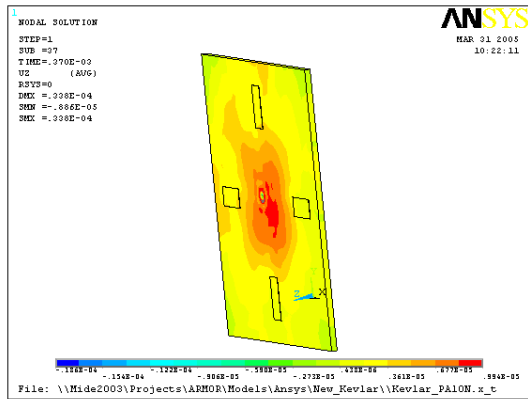
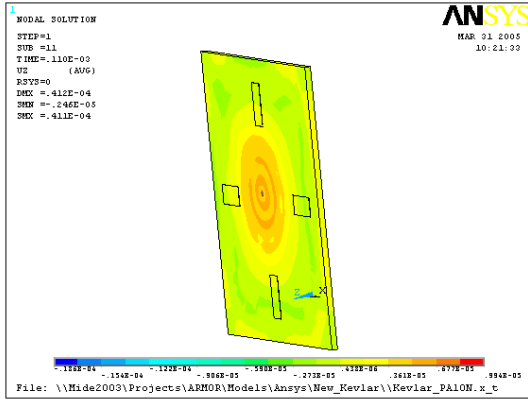
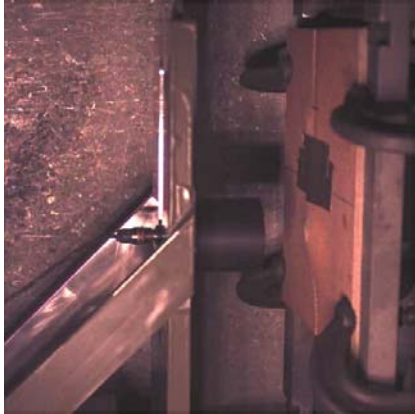


Figure 21. (continued).

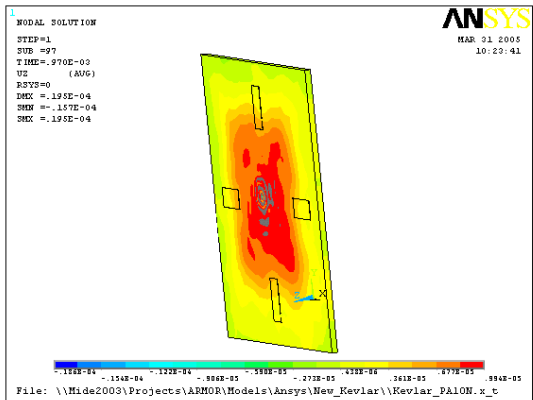
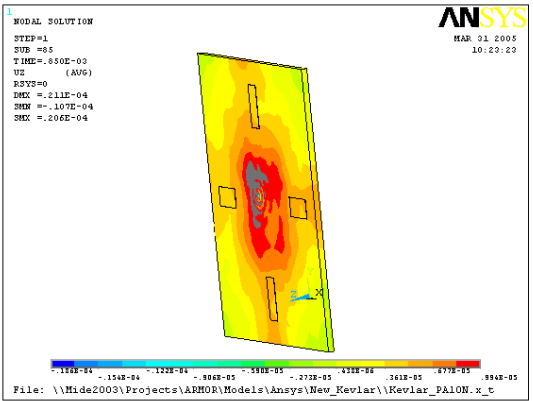
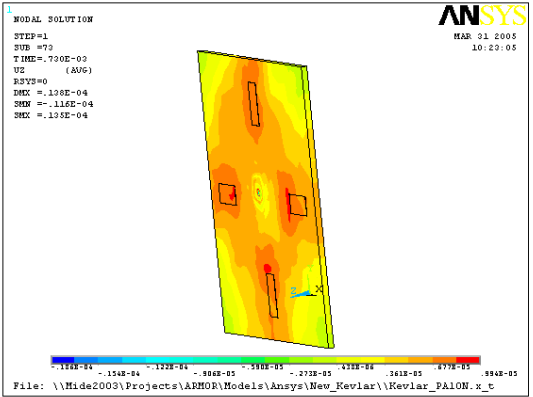


Figure 21. (continued).

1.3.5.3 Voltage Generation Comparison

This section presents a brief comparison between the results obtained from the only good sensor (PA1) in the tests described in section 1.4.2. This sensor was the only one that produced data with some value. A part of the sensor's output is shown in figure 22, where the figure zooms in on the first millisecond of data for comparison with the ANSYS model. The result of the voltage output of the piezo wafer, placed at the same spot as the PA1 sensor is shown in figure 23.

Although the two plots differ in many ways, there are some remarkable resemblances:

- Both have a dominant frequency of ~ 6.5 kHz.
- The maximum voltage for the first peak is ~ 900 V.
- A similar high frequency content is superimposed on the dominant frequency.
- There is a general increase in voltage over the first 1 ms of the event.

Although these similarities are vague, it is encouraging to realize that these similarities exist without the model being calibrated. It may be safe to assume that trends that are identified by the model might be achievable in reality.

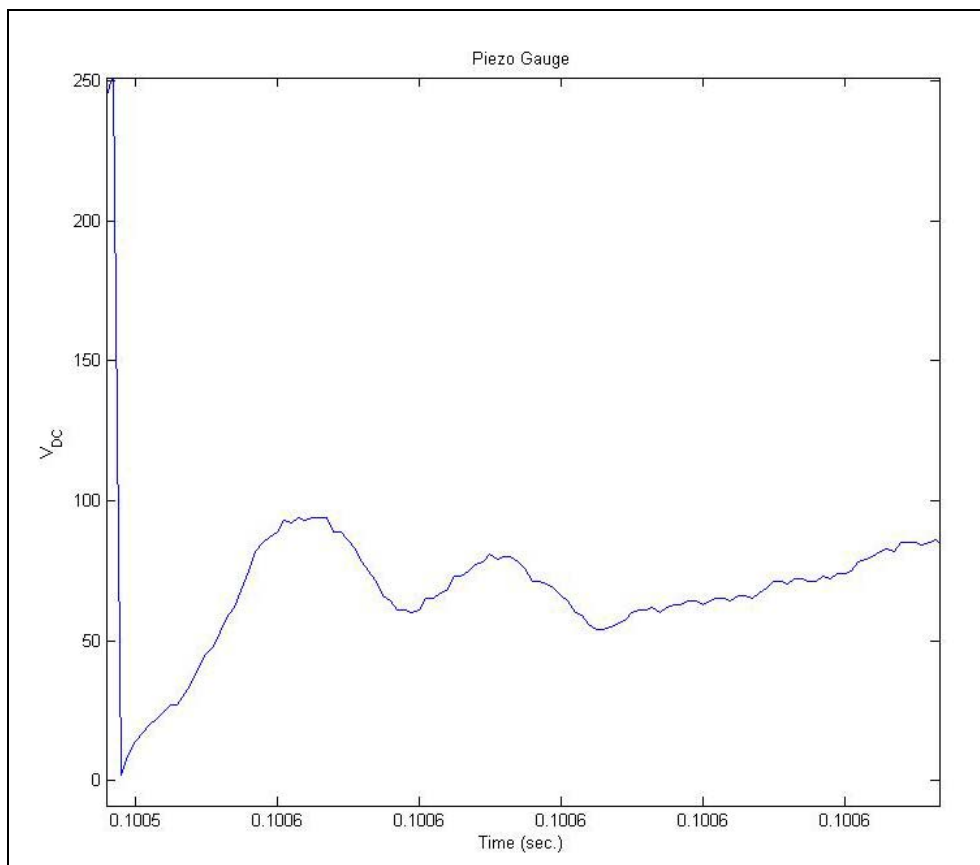


Figure 22. Voltage output from the PA1 piezo sensor during the ballistic test.

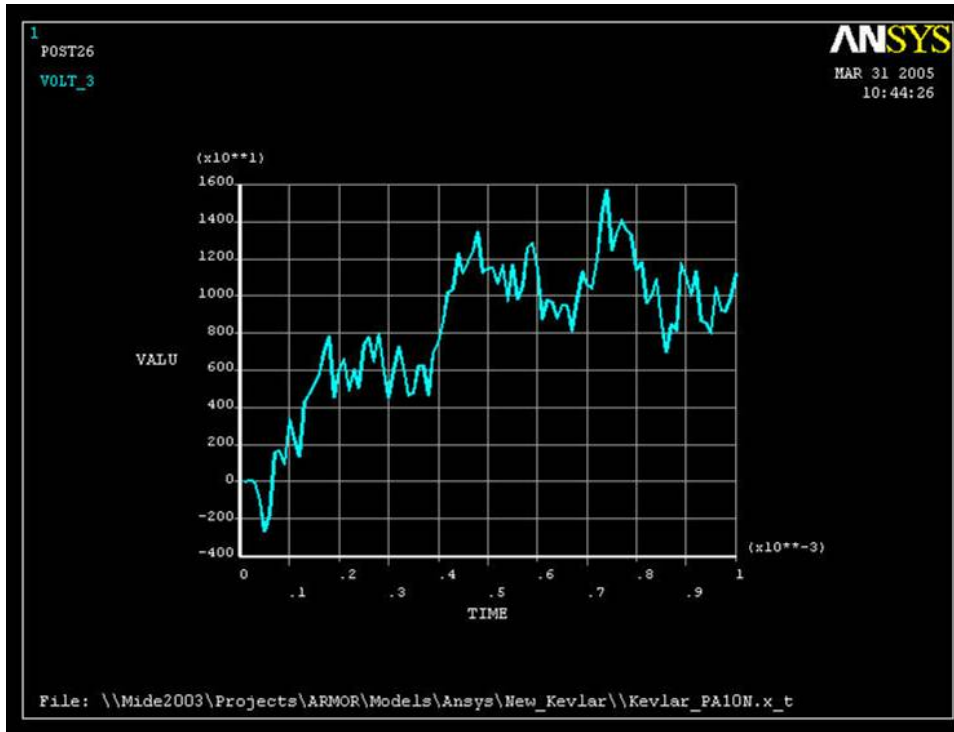


Figure 23. Voltage output from the PA1 piezo sensor in the ANSYS simulation.

1.4 Task 4: Preliminary Experiments

Small experiments were designed and conducted to verify critical elements of the design. The experimental results were used to update and verify the parametric models.

Midé and the ARL decided to combine testing of the baseline Kevlar sheets and preliminary piezoelectric sensor devices. The piezoelectric tests were scheduled for the option, but since the test facilities were available, it was decided to evaluate the piezoelectric devices during a ballistic event and move the design and optimization research to a next phase effort.

1.4.1 Kevlar Plate Tests

Six tests were conducted to determine the displacement of the Kevlar sheets in response to the impact of a high velocity polypropylene bullet.

1.4.1.1 Test Setup

The test setup schematic is shown in figure 24. The controller initiates the event by sending an electric pulse to the gun. This pulse activates the firing pin of the gun and ignites the charge. The charge propels the polypropylene bullet through the gun's barrel (figure 26) and toward the Kevlar target (figure 25). On the way to the target, the bullet passes through the trigger. The trigger sends a signal to the controller that commands the oscilloscope and the laptop (high-speed camera) to start recording. The eddy displacement gauge (figure 26) records the displacement of

the metal strip, and the laptop computer records the sequence of events that follows the impact of the bullet.

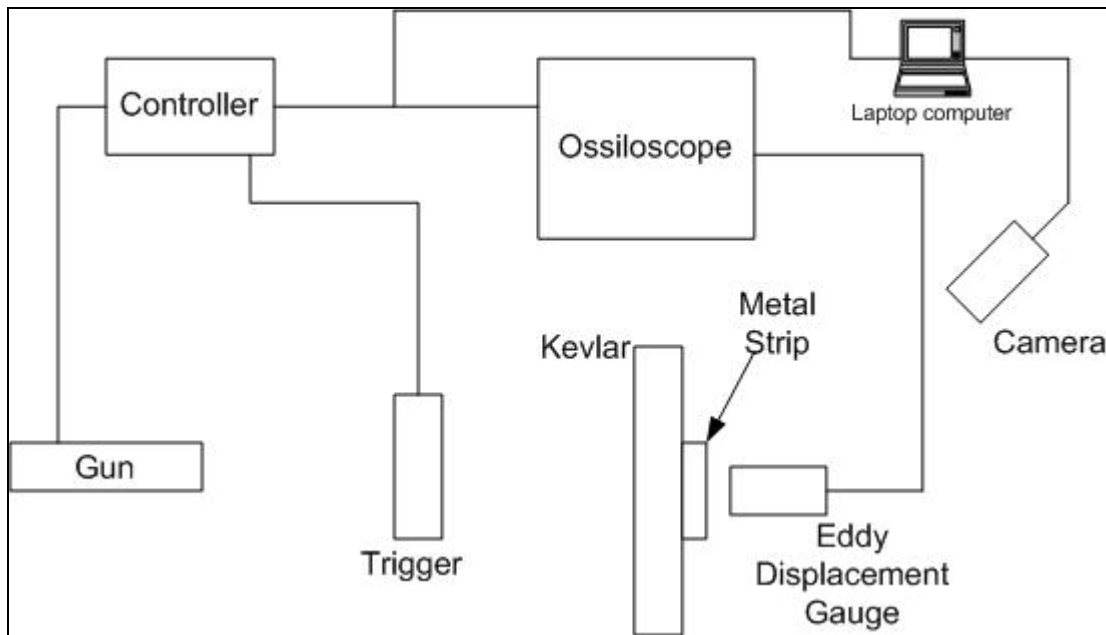


Figure 24. Kevlar displacement test setup.

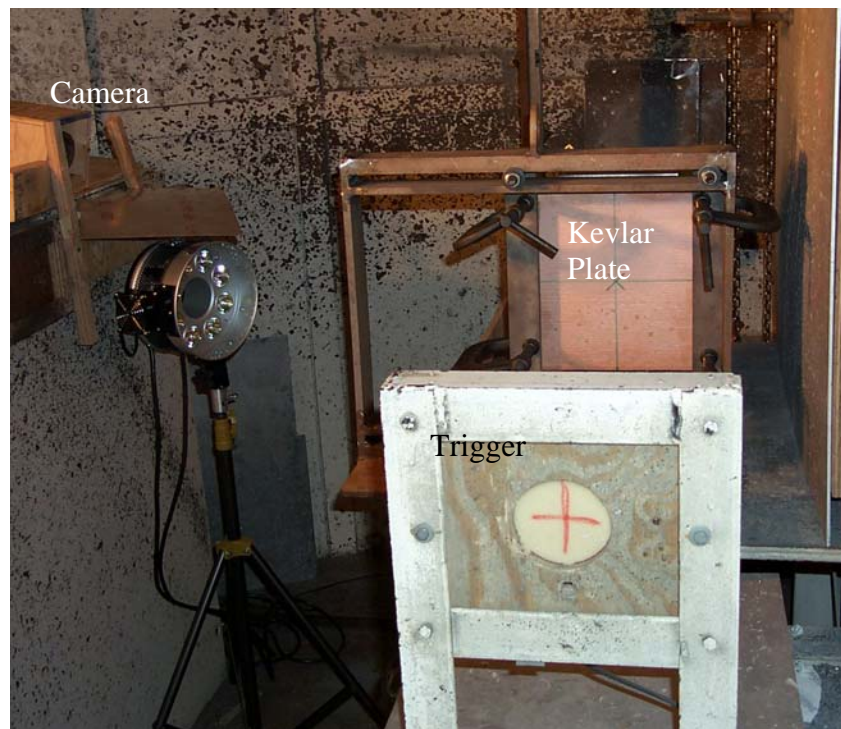


Figure 25. Test setup as viewed from the gun barrel.

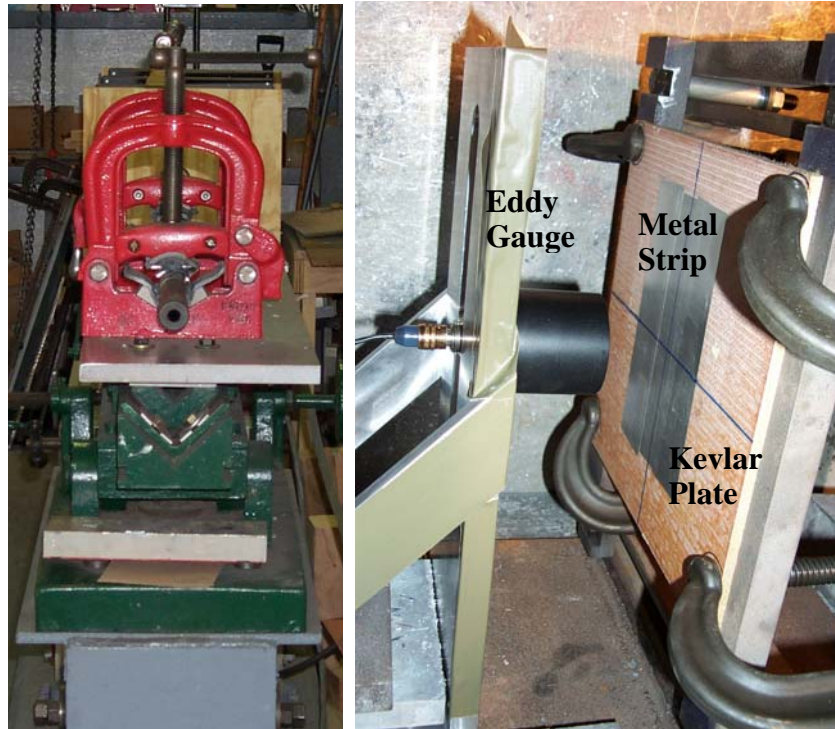


Figure 26. The gun, left and side view of the eddy gauge, metal strip and Kevlar target, right.

1.4.1.2 Test Sequence

Five tests were performed on the bare Kevlar sheets. Unfortunately, the metal strips used were not able to withstand the ballistic event. Only limited data from these tests were available, but none of them were useful to calibrate the model. Additional tests were mostly conducted in an attempt to improve the performance of the metal strips so that displacement data could be recorded.

Table 2 summarizes the tests that were performed at APG. These tests can be divided into the displacement and piezo tests. The displacement tests were the originally scheduled tests for this part of the program. The results from these tests were to be used for the calibration of the FEA model. As stated before, the tests ended mostly in the destruction of the metal pieces needed by the measuring equipment, and thus, no usable data were obtained from them.

Figures 27 to 32 show the failures of the different tests. Initially, the metal strips for the eddy current gauge were bonded to a protective layer that covered the Kevlar plate. The existence of this layer was only discovered after test 2647. Although this layer was removed for the subsequent tests, the bonding layer between the metal and the Kevlar was not strong enough to withstand the ballistic event. Ensuing tests will have the metal integrated with the Kevlar and this should solve the problem. The QuickPack and PowerAct tests produced some useful data and these tests are described in some more detail next.

Table 2. Test sequence and failure mechanisms for a ballistic test conducted at ARL.

Test No.	Description	Failure Mechanism
2646	Displacement test. Three 2-inch metal tape strips	Metal tape ruptures
2647	Displacement test. Metal sheet bonded to structure	Metal sheet ruptures
2648	Displacement test; 0.75-inch-diameter metal tape placed under the impact point.	Metal disc intact; data not useful for calibration of model.
2649	Displacement test; 0.75-inch-diameter metal disc bonded to structure.	Disk blown off structure.
2650	Displacement test; 0.75-inch-diameter thin metal disc bonded to structure	Thin disk blown off structure.
2651	Multi layer piezo test.	Piezos bonded to protective layer. Piezos delaminated from structure.
2652	QuickPack and PowerAct piezo wafer test.	Sensors bonded to protective layer. QuickPacks failed structurally. One PowerAct intact.



Figure 27. Setup before test number 2646.



Figure 28. Failure during test 2646. (Note how the tape tears in all directions, indicating severe strain-related failure of the metal.)



Figure 29. Failure of test 2647. (Again, the rupture of the metal sheet indicated that the strain limit of the material was exceeded significantly.)



Figure 30. The impact point is well above the position of the 0.75-inch metal disk in test 2648. (The impact does not dislodge the tape, indicating that a smaller area might have a chance of surviving the high differential strain environment of the ballistic test.)

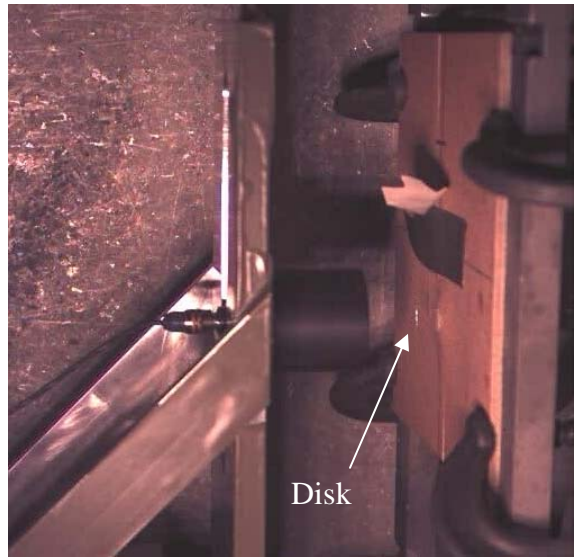


Figure 31. Delaminating of the 0.75-inch metal disk during test 2649.



Figure 32. Failure of test 2650 was attributable to the dislodging of the metal disk.

1.4.2 Integrated Piezo Tests

Although tests with piezoelectric elements are part of the option for this program, Midé decided to combine these tests with the Kevlar plate tests. The main reason for this is to fail early and learn lessons in order to succeed later. In order to accomplish this, two sets of piezoelectric sensors and actuators were bonded to the Kevlar surface. As stated earlier, the surface was covered with a “peel-off” protective layer, the existence of which was only discovered during the tests at ARL. Thus, the piezoelectric materials were actually bonded to the protective peel-off layer.

Two Kevlar plates were instrumented with piezos for tests 2651 and 2652. The first set of piezo-electric elements consisted of four layers of piezoelectric arrays. Each layer consisted of six rows of piezos that were made from three separate 1.8-inch by 0.83-inch by 0.006-inch piezoelectric wafers, coupled in parallel to each other. The second set of piezos consisted of two sets of Midé’s PA10N PowerAct and QP10N QuickPack actuators. The description and summary of the tests are given in table 3.

Table 3. Description of the integrated piezo tests.

Test No.	Description	Failure Mechanism
2651	Multi layer piezo test.	Piezors bonded to protective layer. Piezos delaminated from structure.
2652	QuickPack and PowerAct piezo wafer test.	Sensors bonded to protective layer. QuickPacks failed structurally. One PowerAct intact.

Because of the presence of the protective layer, the initial shock was enough to remove the piezos from the Kevlar, and no useful data were obtained. It is not deemed necessary to describe the test and the configurations or the results at any length.



Figure 33. Four layers of piezoelectric elements with various electric configurations were bonded to the target as shown on the left. (Unfortunately, because of the presence of a protective layer, the piezos were not bonded to the structure and the failure [right] resulted during test 2651. No useful data were obtained.)

The second piezo tests had four encapsulated piezoelectric wafers bonded to the Kevlar plate. The test setup is shown in figure 34. Two QuickPack QP10Ns and PowerAct PA10Ns were placed opposite each other as shown. The details of the sensors are listed in table 4. A short description of the two types of actuators is available at <http://www.mide.com>.

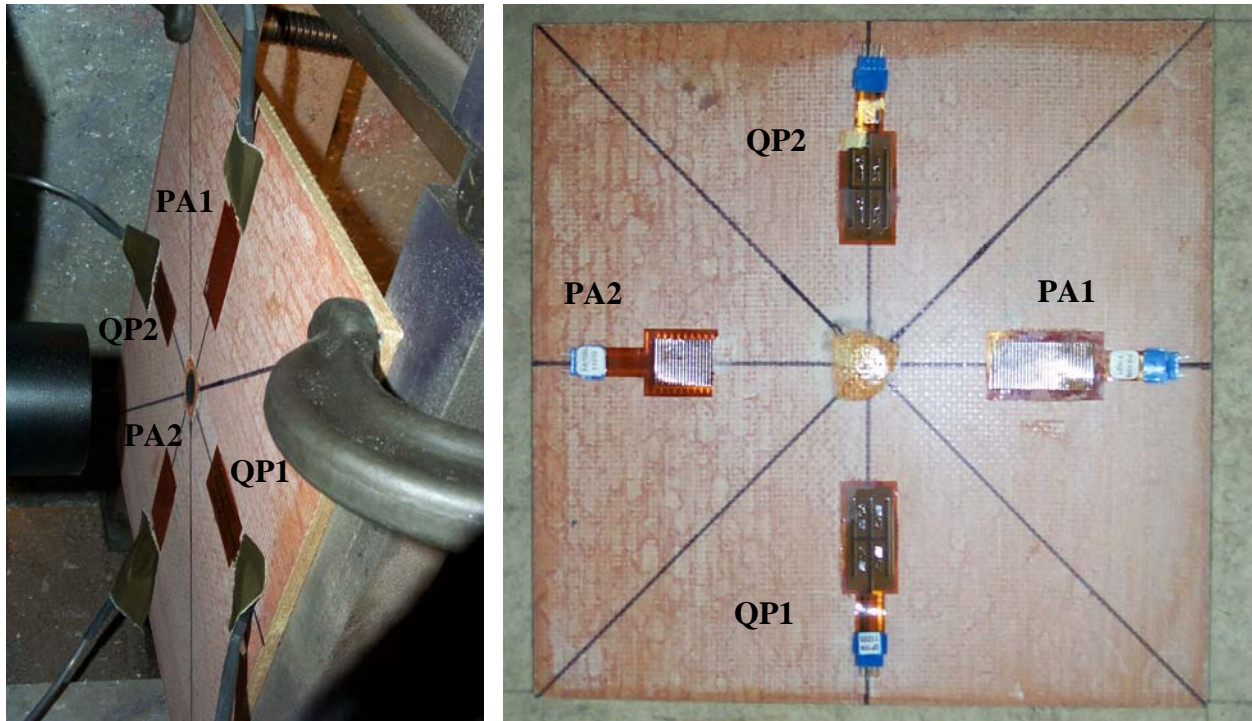


Figure 34. Pre- and post-test 2652 pictures of the QuickPack and PowerAct sensors.

Table 4. Details of the four encapsulated piezoelectric wafers bonded to the Kevlar plate.

Sensor No.	Description	Wafer Size (in.)	Serial No.	Piezo Material	Capacitance (nF)
PA1	Conformable wafer	1.83 x .83 x 0.01	PA11201	PZT5A	41.7
PA2	Conformable wafer	1.83 x .83 x 0.01	PA11010	PZT5A	45
QP1	Rigid wafer	1.83 x .83 x 0.01	QP11205	PZT5A	54.4
QP2	Rigid wafer	1.83 x .83 x 0.01	QP11214	PZT5A	52.6

Although the wafers were bonded to the protective layer, some useful data were obtained from the sensors. These results are shown in figures 35 through 39 and were used in the modeling section to compare with the predicted output from the sensors. The picture on the left of figure 34 shows the effect that the ballistic event had on the sensors. PA1 is the only sensor that remained intact. All the other sensors were destroyed by the event. It was expected that the high strains would crack the rigid QuickPacks. The failure of the one PowerAct can only be explained by the fact that it was bonded to the protective layer, which delaminated during the event, causing the PowerAct to be accelerated away from the surface and to experience abnormal bending.

Figure 35 shows the results from the eddy current gauge. The 0.75-inch metal strip was removed from the Kevlar plate by the ballistic event. This caused a spike in the gauge data and indicated the time of impact. No further useful data can be derived from the signal.

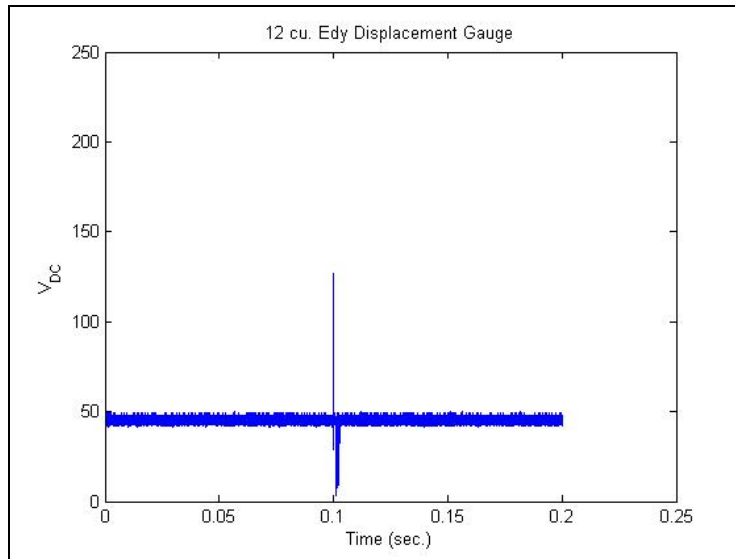


Figure 35. Results from the eddy current gauge. (This result is indicative of the failure of the metal strip to remain on the Kevlar composite plate. However, it indicated the initial event at 0.1 sec after trigger, which is useful for analysis of the piezoelectric signals.)

Figure 36 shows the signal obtained from PA1. This is the only useful piece of data available from the entire test series. This trace was further analyzed in the modeling section where it was compared with the ANSYS model. Here, we can note a few features of the signal. The first resonant mode is at 140 Hz. The initial impact is sensed but does not drive the signal to the limit. The shock arriving around 0.01 second after impact drives the signal out of range, indicating that this is the main event.

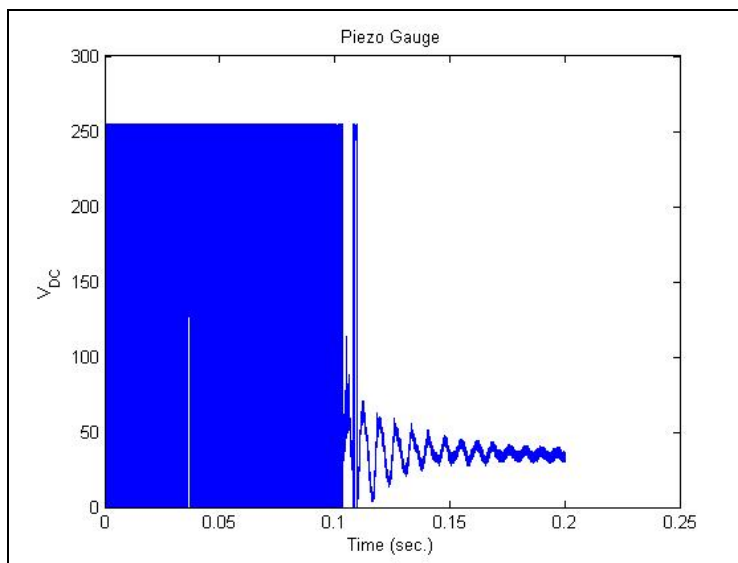


Figure 36. Output from PA1. (The continuous trace after the event indicates that these are useful data. The spike at 0.11 sec exceeded the limits of the oscilloscope.)

Figure 37 shows the result from QP1. The impact cracked the piezo into a number of smaller pieces. The data show this as the different, disconnected pieces generate their individual signals that are combined in the trace. This combined signal appears as a random trace, as can be seen in figure 37.

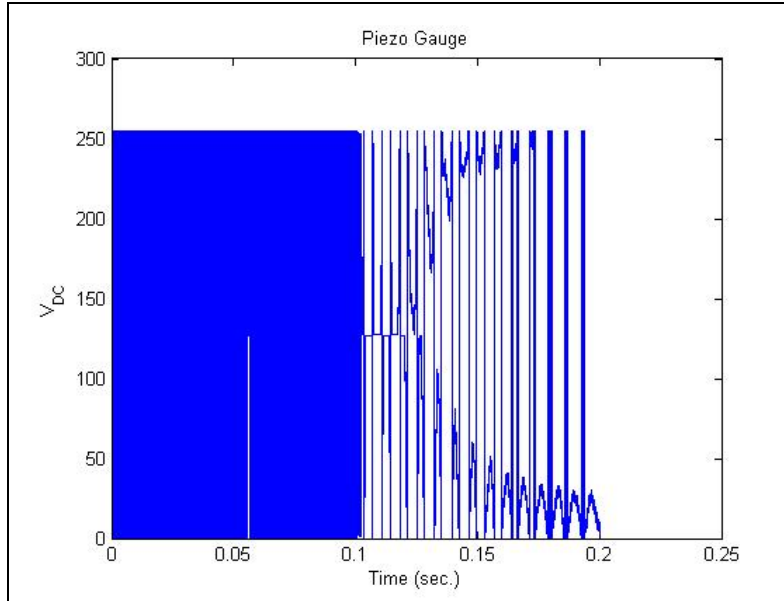


Figure 37. Output from QP1. (It is clear that the sensor produced random signal because the wafer was cracked.)

Figures 38 and 39 show what happens when the wafer becomes dislodged from the Kevlar. The ballistic wave pushes the piezo, having momentum, back. This causes the element to bend and completely break off, as can be seen in the left picture of figure 34. The output voltage traces from the elements indicate an initial charge that then bleeds off after the piezo is destroyed.

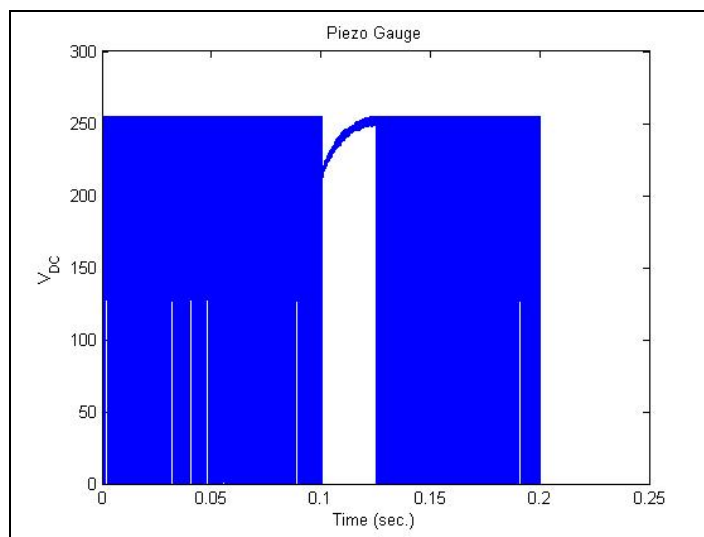


Figure 38. Output from PA2. (The sensor breaks immediately after the initiating event, bleeding its charge to the oscilloscope.)

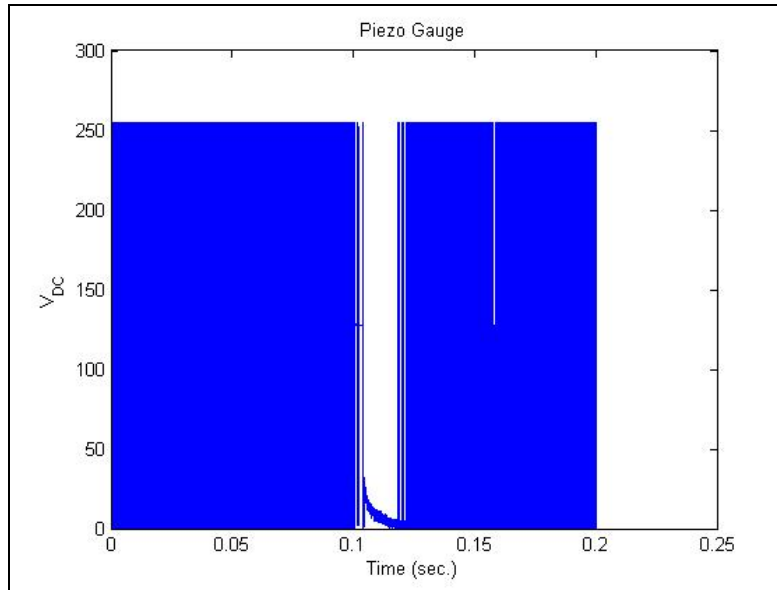


Figure 39. Output from QP2. (This sensor also has a catastrophic failure, thus the bleed-off of the initial signal.)

1.5 Task 5: Shock Absorber Design

With the parametric model developed in Task 2 and updated in Task 4, design a detailed sandwiched piezoelectric shock absorption system that can be fabricated and tested in the option.

The ANSYS model was used to determine the effect of sending a high voltage pulse to piezo wafers that were placed around the impact point in order to create a disturbance wave. It was hypothesized that this disturbance wave might reduce the displacement of the cone at the impact point and thus diminish injuries and damage during a ballistic event.

The model was used to simulate the effect that 0.5-inch-thick piezo wafers might have on the displacement of the Kevlar composite plate. It is common practice to limit the electric field in a piezo to 20 V/mil. This was the maximum field that was used in the model. Again, the initial conditions of the model were to constrain the corners of the Kevlar plate to zero movement and to add an initial velocity of 1000 m/s to the node in a 0.5-inch diameter around the center of the plate. Two simulations were run, one with the voltage pulse and one without for comparison.

Figure 40 shows the displacement of the center node only in response to the ballistic event. The node is displaced a maximum of 230 micro-strains 0.38 ms after bullet impact. Figure 41 shows the displacement of the same node, but this time with a destructive wave generated by the piezos. The maximum displacement is 180 micro-strains 0.39 ms after the ballistic event. This is a 27% reduction in displacement. It is further interesting to note the high frequency element present in the piezo-actuated simulation. This high frequency element can be responsible for the reduction in the center node amplitude.

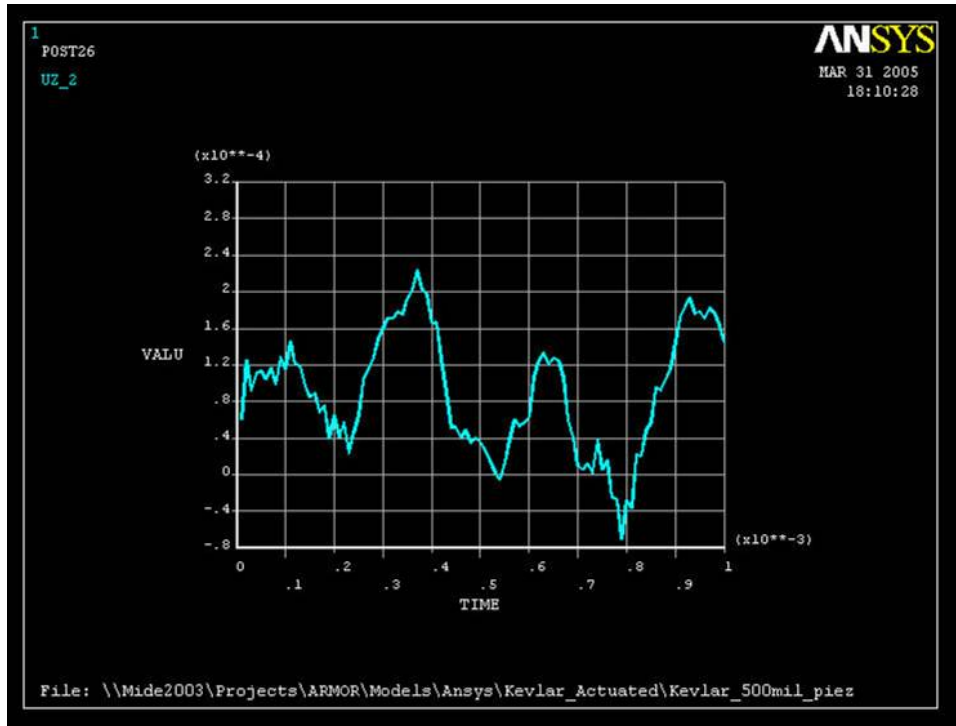


Figure 40. Displacement of the center node in response to the ballistic event.

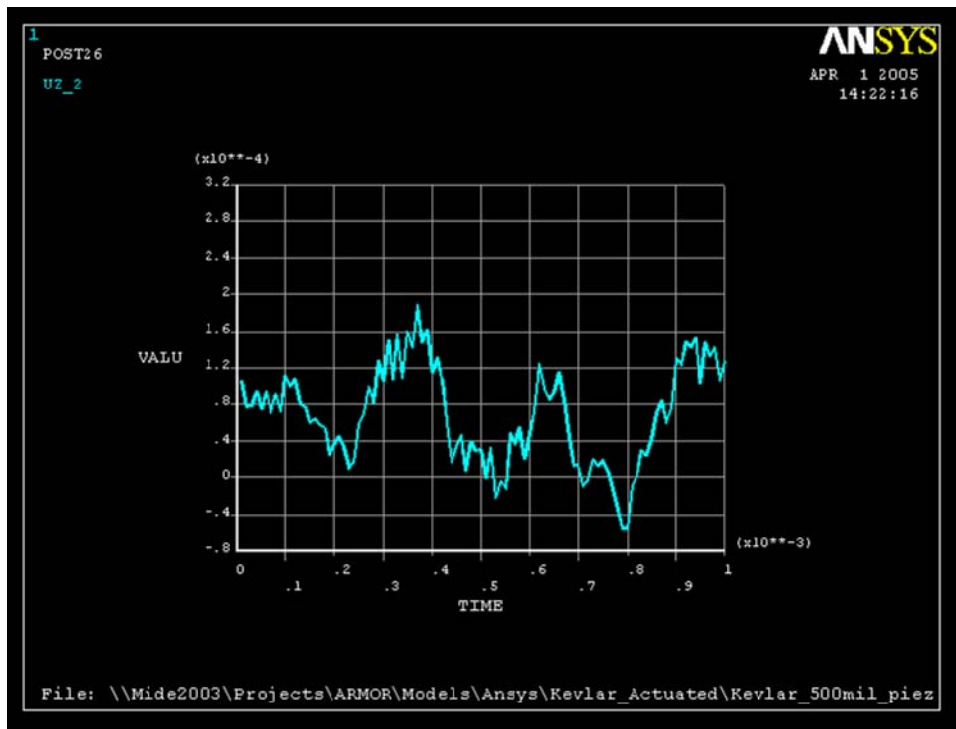


Figure 41. Displacement of the center node in response to the ballistic event when a structural interference wave is generated by the piezoelectric elements in response to a high voltage pulse.

These are encouraging results, but caution must be exercised. The actual meaning of the displacement units can only be determined when the model is calibrated. This calibration, and only this calibration, will quantify these results.

Once the model is calibrated, the ANSYS model can be used to find the best way to reduce the displacement of the center node. The model is now set up so that the following variables can easily be changed in order to find the optimal solution:

- Piezo size
- Piezo placement
- Electric field
 - Waveform
 - Amplitude
- Piezo material
- Piezo coupling
- Control scheme

2. Conclusion and Future Work

The option was initially created to build and test a Kevlar composite plate with piezos integrated into the plate. The tests evaluated the optimal solution as determined by the modeling of Phase I. As stated earlier, problems with obtaining reliable data reduced the effectiveness of the modeling in Phase I. Some of the option work was completed by testing integrated piezos, but again, the impact of the tests was reduced by the unavailability of reliable displacement data.

Efforts are under way to improve the displacement data. The models have been created and are ready to be optimized. The period between the end of Phase I and the start of the option will be used to improve the displacement data. This will enable Midé to complete the optimization very early in the option, so that the prototypes can be built and tested without disrupting the program further.

3. References

1. Institute of Electrical and Electronics Engineers. *IEEE Standard on Piezoelectricity*; STD-176-1978; New York, 1978.
2. Straßburger, E.; Senf, H.; Burkins, M. S.; Gooch W. A. Dynamic Impact Resistance of Ceramic-GRP Composite Targets. *Presented at the 16th International Symposium on Ballistics*, San Francisco, CA, September 23-27, 1996.

INTENTIONALLY LEFT BLANK.

Appendix A. MATLAB Main Code

```
% Construct a lumped parameter model of a bullet impact
close all
clear all
pack

% SIMULATION
Delt_Frac=0.02;
% Delt_Frac=0.1;
Nstep=4000;
zeta=2e-10;      % Damping ratio
% zeta=0*1e-17;  % Damping ratio
iplt=1;         % Plot option (0 = No plots)
number_node=0;  % = 1: Plot the node numbers
number_element=0; % = 1: Plot the element numbers
Nskip=20;       % Number of steps between animation plots
Deformation_Scale=1; % Scaling factor for the deformation
Case_Name='APG';
save_opt=1;     % = 1; Save the plots in jpg format
movie_opt=1;    % = 1; Save a movie of the impact response
stress_opt=1;   % Calculate the stresses

% GEOMETRY
Nx = 13;      % Number of elements in the planar direction
Ny = Nx;
Lx = 0.2286;  % Length or width of the armor protection
Nz = 5;      % Number of elements in the thickness direction
Lz = .00635; % Thickness
Ly = Lx;     % Consider a square plate
Ly = Lx;     % Just a strip to better match the stiffness
MidNod=fix(Nx/2);
Iimpact=MidNod+MidNod*Nx+1;
Ibehind=Iimpact + Nx*Ny*(Nz-1);

delx=Lx/(Nx-1);
dely=Ly/(Ny-1);
delz=Lz/(Nz-1);

% BULLET
Bullet_Velocity=600; % Bullet impact velocity
Bullet_Mass=.00156;  % Bullet mass

% MATERIAL PROPERTIES
EyoungXX=24.1E9;
```

```

EyoungYY=24.1E9;
EyoungZZ=10.4E9;
nhuzx=0.12;
nhuyz=0.12;
nhuxy=0.4;
Density=1440;

fprintf('\n Total Mass = %6.2f kg or %6.2f lb \n',Density*Lx*Ly*Lz,Density*Lx*Ly*Lz*2.2);

% Construct the coordinates
ii=0;
for k=1:Nz
    for j=1:Ny
        for i=1:Nx
            ii=ii+1;
            Coord(ii,1)=(i-1)*delx;
            Coord(ii,2)=(j-1)*dely;
            Coord(ii,3)=(k-1)*delz;
        end
    end
end
Nnode=ii;

% Construct the "Nodal" Connectivity
% First in the X-direction
ielem = 0;
for k=1:Nz-1
    for j=1:Ny-1
        for i=1:Nx-1
            ielem = ielem+1;
            Nconec(ielem,1)=(k-1)*Nx*Ny + (j-1)*Nx + i;
            Nconec(ielem,2)=(k-1)*Nx*Ny + (j-1)*Nx + i + 1;
            Nconec(ielem,3)=(k-1)*Nx*Ny + j*Nx + i + 1;
            Nconec(ielem,4)=(k-1)*Nx*Ny + j*Nx + i;
            Nconec(ielem,5)=k*Nx*Ny + (j-1)*Nx + i;
            Nconec(ielem,6)=k*Nx*Ny + (j-1)*Nx + i + 1;
            Nconec(ielem,7)=k*Nx*Ny + j*Nx + i + 1;
            Nconec(ielem,8)=k*Nx*Ny + j*Nx + i;
        end
    end
end
Nelem=ielem;

Alive=ones(Nelem,1);

% Plot the grid on a non-equal axes grid
if(iplt~=0);plot_model_8;end

```

```

NGP = 3;
% Now calculate and construct the finite element model
KMat=sparse(zeros(3*Nnode,3*Nnode));
TMat=sparse(zeros(3*Nnode,3*Nnode));
MMat=sparse(zeros(3*Nnode,1));
for ielem=1:Nelem
    for j=1:8
        XI(j,1) = Coord(Nconec(ielem,j),1);
        YI(j,1) = Coord(Nconec(ielem,j),2);
        ZI(j,1) = Coord(Nconec(ielem,j),3);
    end
    [STIFM1 ,JAC] = ANSTFSOL (XI ,YI ,ZI ,EyoungXX ,EyoungYY ,EyoungZZ ,...
        nhuxy ,nhuyz ,nhuzx ,NGP );
    [EMASS ,JAC ,XCG ,YCG ,ZCG ,TMASS] = MASSOL (XI ,YI ,ZI ,Density ,NGP );

    for i=1:8
        IC = Nconec(ielem,i);
        for k1=1:3
            IC2=(IC-1)*3+k1;
            ICS = (i - 1)*3 + k1;
            for j=1:8
                IR = Nconec(ielem,j);
                for k2=1:3
                    IR2 = (IR - 1)*3 + k2;
                    IRS = (j - 1)*3 + k2;
                    KMat(IR2,IC2) = KMat(IR2,IC2) + Alive(ielem)*STIFM1 (IRS ,ICS );
                end
            end
        end
    end
end

    for i=1:8
        ID = Nconec(ielem,i);
        for k1=1:3
            ID2=(ID-1)*3+k1;
            MMat(ID2) = MMat(ID2) + EMASS (i );
        end
    end
end

for i=1:Nnode*3
    TMat(i,:)=KMat(i,:)/MMat(i);
end
% TMat(1:3,1:3)
[phi,eval]=eig(full(TMat));
[Freq,iord]=sort(sqrt(real(diag(eval)))/(2*pi));
for i=1:Nnode*3

```

```

    phi1(:,i)=phi(:,iord(i));
end
phi=phi1;
clear phi1
delt=Delt_Frac/max(Freq);
fprintf('\n\n Lowest Natural Frequency: %7.3f Hz \n\n',Freq(7));

save Restart TMat KMat MMat phi Freq

wold=zeros(Nnode*3,1);
wvold=zeros(Nnode*3,1);
KE_Bullet=0.5*Bullet_Velocity*Bullet_Velocity*Bullet_Mass;
Imparted_Velocity=sqrt(KE_Bullet*2/(MMat(Iimpact*3) + Bullet_Mass));

wold(Iimpact*3)=Imparted_Velocity*delt;
wvold(Iimpact*3)=0;

MMat(Iimpact*3)=MMat(Iimpact*3) + Bullet_Mass;
MMat(Iimpact*3-1)=MMat(Iimpact*3-1) + Bullet_Mass;
MMat(Iimpact*3-2)=MMat(Iimpact*3-2) + Bullet_Mass;
for i=1:Nnode*3
    TMat(i,:)=KMat(i,:)/MMat(i);
end
wvel=(wold-wvold)/(delt);
% KE0=0.5*wvel'.*MMat'*wvel

if(iplt~=0);plot_deformed_8;end

w_store=zeros(Nstep,Nnode*3);

Nstress=Nstep/Nskip;
VMStress_store=zeros(Nstress,Nelem);
wvel_store=w_store;
istress=0;
for itime=1:Nstep
    Time(itime)=(itime-1)*delt;
    wvel=(wold-wvold)/(delt);
    wnew=+2*wold - wvold - delt*delt*TMat*wold - delt*delt*zeta*TMat*wvel;

    w_store(itime,:)=wnew;
    wvel_store(itime,:)=wvel;
    wvold=wold;
    wold=wnew;

% Calculate the Kinetic Energy
KE(itime)=0.5*wvel'.*MMat'*wvel;
PE(itime)=0.125*(wold+wvold)*KMat*(wold+wvold);

```

```

% Calculate the stresses around the impact point
if(mod(itime,Nskip) == 0);
    fprintf(' Time Step %d \n',itime);
    if (stress_opt == 1)
        istress = istress + 1;
        for ielem=1:Nelem
            for j=1:8
                XI(j,1) = Coord(Nconec(ielem,j),1);
                YI(j,1) = Coord(Nconec(ielem,j),2);
                ZI(j,1) = Coord(Nconec(ielem,j),3);
                U(j*3-2,1) = wnew(Nconec(ielem,j)*3-2);
                U(j*3-1,1) = wnew(Nconec(ielem,j)*3-1);
                U(j*3,1) = wnew(Nconec(ielem,j)*3);
            end
            [SIGX ,SIGY ,SIGZ ,SIGXY ,SIGYZ ,SIGZX ,SIGVM ,JAC] = ...
            ANSTRSOL (XI ,YI ,ZI ,U ,EyoungXX ,EyoungYY ,EyoungZZ ,nhuxy ,nhuyz ,nhuzx ,NGP );
            VMStress_store(istress,ielem)=SIGVM(9)/1E6;    % In MPa
        %     if(ielem==1);
        %         U(1:16)'
        %         VMStress_store(istress,;)
        %         pause
        %     end
        %     if(ielem==4);
        %         U(1:16)'
        %         VMStress_store(istress,;)
        %         pause
        %     end
        end
    end
end
end
end
end

```

```

save Restart TMat KMat MMat phi Freq KE PE wvel_store w_store Time VMStress_store

```

```

figure(2)
subplot(211)
plot(Time,w_store(:,Iimpact*3));xlabel('Time (seconds)');ylabel('Z-Displacement of Impact Point (m)')
subplot(212)
plot(Time,wvel_store(:,Iimpact*3));xlabel('Time (seconds)');ylabel('Z-Velocity of Impact Point (m/s)')
figure(2)

```

```

figure(3)
subplot(211)
plot(Time,w_store(:,Ibehind*3));xlabel('Time (seconds)');ylabel('Z-Displacement of Back (m)')
subplot(212)
plot(Time,wvel_store(:,Ibehind*3));xlabel('Time (seconds)');ylabel('Z-Velocity of Back (m/s)')
figure(3)

```

```
figure(4)
subplot(311)
plot(Time,KE);xlabel('Time (seconds)');ylabel('Kinetic Energy (J)')
subplot(312)
plot(Time,PE);xlabel('Time (seconds)');ylabel('Potential Energy (J)')
subplot(313)
plot(Time,PE+KE);xlabel('Time (seconds)');ylabel('Total Energy (J)')
figure(4)

if(iplt~=0);animate_filled_8;end
```

<u>NO. OF COPIES</u>	<u>ORGANIZATION</u>
1 (PDF ONLY)	DEFENSE TECHNICAL INFORMATION CTR DTIC OCA 8725 JOHN J KINGMAN RD STE 0944 FORT BELVOIR VA 22060-6218
1	US ARMY RSRCH DEV & ENGRG CMD SYSTEMS OF SYSTEMS INTEGRATION AMSRD SS T 6000 6TH ST STE 100 FORT BELVOIR VA 22060-5608
1	DIRECTOR US ARMY RESEARCH LAB IMNE ALC IMS 2800 POWDER MILL RD ADELPHI MD 20783-1197
1	DIRECTOR US ARMY RESEARCH LAB AMSRD ARL CI OK TL 2800 POWDER MILL RD ADELPHI MD 20783-1197
2	DIRECTOR US ARMY RESEARCH LAB AMSRD ARL CS OK T 2800 POWDER MILL RD ADELPHI MD 20783-1197
7	CDR US ARMY TACOM ATTN AMSTA TR S T FURMANIAK S GOODMAN D HANSEN L PROKURAT FRANKS D TEMPLETON D THOMAS AMSTA TR STI J CARIE WARREN MI 48397-5000
1	PROJECT MANAGER ABRAMS TANK SYSTEM ATTN SFAE GCSS W ABS J ROWE WARREN MI 48397-5000
3	CDR US ARMY RSCH OFFICE ATTN J BAILEY K IYER K LOGAN PO BOX 12211 RSCH TRIANGLE PARK NC 27709-2211

<u>NO. OF COPIES</u>	<u>ORGANIZATION</u>
1	CDR NGIC ATTN J CRIDER W GSTATTENBAUER 220 SEVENTH AVENUE CHARLOTTESVILLE VA 22901-5391
1	CRUSADER OPM ATTN SFAE GCSS CR E B ROOPCHAND BLDG 171A PICATINNY ARSENAL NJ 07806-5000
1	CIA ATTN OSWR DSD W WALTMAN RM 5P0110 NHB WASHINGTON DC 20505
1	DIRECTOR DARPA 3701 NORTH FAIRFAX DR ARLINGTON VA 22203-1714
1	PM BFVS ATTN SFAE GCSS W BV S M KING WARREN MI 48397-5000
1	CDR CARDEROCK DIV NSWC ATTN CODE 28 R PETERSON 9500 MACARTHUR BLVD W BETHESDA MD 20817-5700
1	DEPT OF NAVY OFC DIR REPORTING PROG MGR ADVCD AMPHIBIOUS ASSLT D ERDLEY WASHINGTON DC 20380-0001
3	LAWRENCE LIVERMORE NATL LAB ATTN R GOGOLEWSKI L290 R LANDINGHAM L369 J REAUGH L32 PO BOX 808 LIVERMORE CA 94550
2	LOS ALAMOS NATL LAB ATTN F ADDESSIO M BURKETT LOS ALAMOS NM 87545
1	NAVAL RSCH LABORATORY ATTN CODE 6684 4555 OVERLOOK AVE SW WASHINGTON DC 20375

<u>NO. OF COPIES</u>	<u>ORGANIZATION</u>
5	SANDIA NATL LAB ATTN J ASAY MS 0548 R BRANNON MS 0820 L CHHABILDAS MS 0821 D CRAWFORD ORG 0821 M FORRESTAL DIV 1551 PO BOX 5800 ALBUQUERQUE NM 87185-0307
1	AIR FORCE ARMAMENT LAB ATTN AFATL DLJW W COOK EGLIN AFB FL 32542
4	INST FOR ADVNCD TECH ATTN S BLESS H FAIR D LITTLEFIELD R SUBRAMANIAN 3925 W BRAKER LANE STE 400 AUSTIN TX 78759-5316
1	UNIV OF DAYTON RSCH INST ATTN KLA14 N BRAR 300 COLLEGE PARK DAYTON OH 45469-0182
3	SOUTHWEST RSCH INST ATTN C ANDERSON J RIEGEL J WALKER 6220 CULEBRA RD SAN ANTONIO TX 78238
4	US DEPT OF ENERGY ALBANY RSCH CENTER ATTN J HANSEN (2 CYS) P TURNER (2 CYS) 1450 QUEEN AVE SW ALBANY OR 97321-2198
1	BROWN UNIV DIV OF ENGINEERING ATTN R CLIFTON PROVIDENCE RI 02912
2	UNIV OF CA SAN DIEGO DEPT OF APPL MECH & ENGR SVC R011 ATTN S NEMAT NASSER M MEYERS LA JOLLA CA 92093-0411
1	ARMORWORKS ATTN W PERCIBALLI 1701 W 10TH ST STE 5 TEMPE AZ 85281

<u>NO. OF COPIES</u>	<u>ORGANIZATION</u>
2	AERONAUTICAL RSCH ASSN ATTN R CONTILIANO J WALKER PO BOX 2229 50 WASHINGTON RD PRINCETON NJ 08540
1	ALLIANT TECHSYSTEMS INC ATTN G JOHNSON 5050 LINCOLN DR MINNEAPOLIS MN 55436-1097
1	APPLIED RSCH ASSN INC ATTN J YATTEAU 5941 S MIDDLEFIELD RD STE 100 LITTLETON CO 80123
1	APPLIED RSCH ASSN INC ATTN D GRADY 4300 SAN MATEO BLVD NE STE A 220 ALBUQUERQUE NM 87110
1	BRIGGS COMPANY ATTN J BACKOFEN 2668 PETERSBOROUGH ST HERNDON VA 222071-2443
2	CENTURY DYNAMICS INC ATTN B GERBER N BIRNBAUM 2333 SAN RAMON VALLEY BLVD SAN RAMON CA 94583-1613
3	CERCOM ATTN R PALICKA G NELSON B CHEN 1960 WATSON WAY VISTA CA 92083
1	CYPRESS INTERNTL ATTN A CAPONECCHI 1201 E ABINGDON DR ALEXANDRIA VA 22314
1	RJ EICHELBERGER 409 W CATHERINE ST BEL AIR MD 21014-3613
1	EPSTEIN AND ASSN ATTN K EPSTEIN 2716 WEMBERLY DR BELMONT CA 94002
1	GENERAL RSCH CORP PO BOX 6770 SANTA BARBARA CA 93160-6770

<u>NO. OF COPIES</u>	<u>ORGANIZATION</u>
2	GALT ALLOYS INC ATTN S FELLOWS S GIANGIORDANO 122 CENTRAL PLAZA N CANTON OH 44702
3	GDLS ATTN W BURKE MZ436 21 24 G CAMPBELL MZ436 30 44 D DEBUSSCHER MZ436 20 29 38500 MOUND RD STERLING HTS MI 48310-3200
3	GDLS ATTN J ERIDON MZ436 21 24 W HERMAN MZ435 01 24 S PENTESCU MZ436 21 24 38500 MOUND RD STERLING HTS MI 48310-3200
1	INTERNATL RSCH ASSN ATTN D ORPHAL 4450 BLACK AVE PLEASANTON CA 94566
1	JET PROPULSION LAB IMPACT PHYSICS GROUP ATTN M ADAMS 4800 OAK GROVE DR PASADENA CA 91109-8099
1	KAMAN SCIENCES CORP 1500 GARDEN OF THE GODS RD COLORADO SPRINGS CO 80907
3	OGARA HESS & EISENHARDT ATTN G ALLEN D MALONE T RUSSELL 9113 LE SAINT DR FAIRFIELD OH 45014
2	ALLVAC OREMET FACILITY ATTN J KOSIN B MAHONEY 530 34TH AVE SW PO BOX 460 ALBANY OR 97321
4	POULTER LABORATORY SRI INTERNATIONAL ATTN D CURRAN R KLOOP L SEAMAN D SHOCKEY 333 RAVENSWOOD AVE MENLO PARK CA 94025

<u>NO. OF COPIES</u>	<u>ORGANIZATION</u>
1	RMI TITANIUM CO ATTN W LOVE 3350 BIRCH STE 210 BREA CA 92821-6267
6	RMI TITANIUM CO ATTN J BENNETT E CHRIST F JANOWSKI W PALLANTE S ROBERTSON O YU 1000 WARREN AVE NILES OH 44446
1	TIMET ATTN J FANNING PO BOX 2128 HENDERSON NV 89009
1	TIMET ATTN J BARBER 1999 BROADWAY STE 4300 DENVER CO 80202
1	SAIC ATTN J FURLONG MS 264 1710 GOODRIDGE DR MCLEAN VA 22102
2	SIMULA INC ATTN R WOLFFE 10016 SOUTH 51ST ST PHOENIX AZ 85044
7	UNITED DEFENSE LP ATTN J DORSCH V HORVATICH B KARIYA M MIDDIONE R MUSANTE R RAJAGOPAL D SCHADE PO BOX 367 SANTA CLARA CA 95103
3	UNITED DEFENSE LP ATTN E BRADY R JENKINS J JOHNSON PO BOX 15512 YORK PA 17405-1512
1	ZERNOW TECH SVCS INC ATTN L ZERNOW 425 W BONITA AVE STE 208 SAN DIMAS CA 91773
5	MIDÉ TECHNOLOGY CORPORATION ATTN M VAN SCHOOR 200 BOSTON AVENUE SUITE 1000 MEDFORD MA 02155

NO. OF
COPIES ORGANIZATION

1 APPLIED RSCH LAB
ACOUSTICS PROGRAM
ATTN D SWANSON
504L APPLIED SCI BLDG
UNIVERSITY PK PA 16803

3 RITA JONES
80 PALISADE AVE
WHITE PLAINS NY 10607

3 TIAX LLC
ATTN JACOB PRETORIUS
15 ACORN PARK
CAMBRIDGE MA 02140

ABERDEEN PROVING GROUND

1 DIRECTOR
US ARMY RSCH LABORATORY
ATTN AMSRD ARL CI OK (TECH LIB)
BLDG 4600

1 DIR USA EBCC
ATTN SCBRD RT
5183 BLACKHAWK RD
APG EA MD 21010-5424

1 CDR USA SBCCOM
ATTN AMSCB CII
5183 BLACKHAWK RD
APG EA MD 21010-5424

2 DIR USAMSAA
ATTN AMXSY D
 AMXSY MP H COHEN
BLDG 392

3 CDR USATEC
ATTN STEAC LI LV E SANDERSON
 M SIMON (2 CYS)
BLDG 400

35 DIRECTOR
US ARMY RSCH LABORATORY
ATTN AMSRD ARL WM T WRIGHT
 AMSRD ARL WM TA M BURKINS
 C HOPPEL E HORWATH
 T JONES (6 CYS) D KLEPONIS
 B LEAVY J RUNYEON
 S SCHOENFELD
 AMSRD ARL WM TB R SKAGGS
 AMSRD ARL WM TC R ANDERSON
 T FARRAND K KIMSEY
 D SCHEFFLER S SCHRAML
 AMSRD ARL WM TD S BILYK
 T BJERKE D CASEM
 J CLAYTON D DANDEKAR
 M GREENFIELD Y HUANG
 K IYER B LOVE H MEYER
 R MUDD E RAPACKI
 M RAFTENBERG M SCHIEDLER
 S SEGLETES T WEERASOORIYA
 AMSRD ARL WM MD B CHEESEMAN

NO. OF
COPIES ORGANIZATION

FOREIGN ADDRESSES

1 EMBASSY OF AUSTRALIA
COUNSELLOR DEFENCE SCIENCE
1601 MASSACHUSETTS AVE NW
WASHINGTON DC 20036-2273

3 AERONAUTICAL & MARITIME RSCH LAB
N MURMAN S CIMPOERU D PAUL
PO BOX 4331
MELBOURNE VIC 3001
AUSTRALIA

1 ARMSCOR
L DU PLESSIS
PRIVATE BAG X337
PRETORIA 0001
SOUTH AFRICA

1 BATTELLE INGENIEURTECHNICK GMBH
W FUCKE
DUESSELDORFFER STR 9
D 65760 ESCHBORN
GERMANY

1 DEFENCE RSCH AGENCY
FORT HALSTEAD SEVEN OAKS
KENT TN14 7BP
UNITED KINGDOM

1 CARLOS III UNIV OF MADRID
C NAVARRO
ESCUELA POLTEENICA SUPERIOR
C/. BUTARQUE 15
28911 LEGANES MADRID
SPAIN

1 CELIUS MATERIAL TEKNIK
KARLSKOGA AB
L HELLNER
S 691 80 KARLSKOGA
SWEDEN

3 CENTRE D'ETUDES GRAMAT
J CAGNOUX C GALLIC
J TRANCHET
GRAMAT 46500
FRANCE

1 MINISTRY OF DEFENCE
DGA DSP STTC G BRAULT
4 RUE DE LA PORTE D'ISSY
00460 ARMEES
F 75015 PARIS
FRANCE

NO. OF
COPIES ORGANIZATION

1 CONDAT
J KIERMEIR
MAXILLANSTR 28
8069 SCHEYERN FERNHAG
GERMANY

2 DEFENCE PROCUREMENT AGCY
G LAUBE W ODERMATT
BALLISTICS WPNS & COMBAT
VEHICLE TEST CTR
CH 3602 THUN
SWITZERLAND

2 TDW
M HELD
POSTFACH 1340
D 86523 SCHROBENHAUSEN
GERMANY

6 DEFENSE RSCH AGENCY
W CARSON I CROUCH C FREW
T HAWKINS B JAMES B SHRUSBSALL
CHOBHAM LANE
CHERTEY SURREY KT16 OEE
UNITED KINGDOM

1 DEFENCE RSCH ESTAB SUFFIELD
C WEICKERT
BOX 4000
MEDICINE HAT ALBERTA TIA 8K6
CANADA

1 DEFENCE RSCH ESTAB
VALCARTIER ARMAMENTS DIV
R DELAGRAVE
2459 PIE X1 BLVD N
PO BOX 8800
CORCELETTE QUEBEC GOA 1RO
CANADA

2 DEUTSCH FRANZOSISCHES
FORSCHUNGSINSTITUT ST LOUIS
H ERNST H LERR
CEDEX 5 RUE DU
GENERAL CASSAGNOU
F 68301 SAINT LOUIS
FRANCE

1 DIEHL GMBH AND CO
M SCHILDKNECHT
FISCHBACHSTRASSE 16
D 90552 ROTBENBACH AD
PEGNITZ
GERMANY

NO. OF
COPIES ORGANIZATION

- 1 DYNAMEC RSCH AB
A PERSSON
PO BOX 201
S 151 23 SODERTALJE
SWEDEN
- 2 ETBS DSTI
P BARNIER M SALLES
ROUTE DE GUERAY
BOITE POSTALE 712
18015 BOURGES CEDEX
FRANCE
- 1 FEDERAL MINISTRY OF DEFENCE
DIR OF EQPT & TECH LAND
RUV 2
D HAUG
POSTFACH 1328
53003 BONN
GERMANY
- 4 FRANHOFER INSTITUT FUR
KURZZEITDYNAMIK
ERNST MACH INSTITUT
V HOHLER E STRASSBURGER
R THAM K THOMA
ECKERSTRASSE 4
D 79 104 FREIBURG
GERMANY
- 1 MINISTRY OF DEFENCE
DGA/SPART
C CANNAVO
10 PLACE GEORGES CLEMENCEAU
BP19
F 92211 SAINT CLOUD CEDEX
FRANCE
- 2 HIGH ENERGY DENSITY RSCH CTR
V FORTOV G KANEL
IZHORSKAY STR 13/19
MOSCOW 127412
RUSSIAN REPUBLIC
- 1 INGENIEURBURO DEISENROTH
F DEISENROTH
AUF DE HARDT 33 35
D 5204 LOHMAR 1
GERMANY
- 1 INST OF CHEMICAL PHYSICS
S RAZORENOV
142432 CHERNOGOLOVKA
MOSCOW REGION
RUSSIAN REPUBLIC

NO. OF
COPIES ORGANIZATION

- 7 INST FOR PROBLEMS IN MATERIALS SCI
S FIRSTOV B GALANOV O GRIGORIEV
V KARTUZOV V KOVTUN Y MILMAN
V TREFILOV
3 KRHYZHANOVSKY STR
252142 KIEV 142
UKRAINE
- 1 INST FOR PROBLEMS
OF STRENGTH
G STEPANOV
TIMIRY AZEVSKAYA STR 2
252014 KIEV
UKRAINE
- 3 INST OF MECH ENGR PROBLEMS
V BULATOV D INDEITSEV
Y MESHCHERYAKOV
BOLSHOY 61 VO
ST PETERSBURG 199178
RUSSIAN REPUBLIC
- 2 IOFFE PHYSICO TECH INST
E DROBYSHEVSKI A KOZHUSHKO
ST PETERSBURG 194021
RUSSIAN REPUBLIC
- 1 K&W THUN
W LANZ
ALLMENDSSTRASSE 86
CH 3602 THUN
SWITZERLAND
- 1 R OGORKIEWICZ
18 TEMPLE SHEEN
LONDON SW 14 7RP
UNITED KINGDOM
- 1 MAX PLANCK INSTITUT FUR
EISENFORSCHUNG GMBH
C DERDER
MAX PLANCK STRASSE 1
40237 DUSSELDORF
GERMANY
- 2 NATL DEFENCE HDQRTRS
PMO MRCV MAJ PACEY
PMO LAV A HODAK
OTTOWA ONTARIO KIA OK2
CANADA

NO. OF
COPIES ORGANIZATION

- 1 OTO BRED
M GUALCO
VIA VALDIOCCHI 15
I 19136 LA SPEZIA
ITALY
- 5 RAPHAEL BALLISTICS CTR
M MAYSELESS Y PARTOM
G ROSENBERG Z ROSENBERG
Y YESHURUN
BOX 2250
HAIFA 31021
ISRAEL
- 1 ROYAL MILITARY ACADEMY
E CELENS
RENAISSANCE AVE 30
B 1040 BRUSSELS
BELGIUM
- 1 ROYAL NETHERLANDS ARMY
J HOENEVELD
V D BURCHLAAN 31
PO BOX 90822
2509 LS THE HAGUE
NETHERLANDS
- 1 DEFENCE MATERIEL ADMIN
WEAPONS DIRECTORATE
A BERG
S 11588 STOCKHOLM
SWEDEN
- 2 SWEDISH DEFENCE RSCH ESTAB
DIVISION OF MATERIALS
S J SAVAGE J ERIKSON
S 172 90 STOCKHOLM
SWEDEN
- 3 SWEDISH DEFENCE RSCH ESTAB
L HOLMBERG B JANZON
P LUNDBERG
BOX 551
S 147 25 TUMBA
SWEDEN
- 1 TECHNION INST OF TECH
FACULTY OF MECH ENGINEERING
S BODNER
TECHNION CITY
HAIFA 32000
ISRAEL

NO. OF
COPIES ORGANIZATION

- 3 TECHNISCHE UNIVERSITAT
CHEMNITZ ZWICKAU
A SCHROEDTER L KRUEGER
L MEYER
POSTFACH
D 09107 CHEMNITZ
GERMANY
- 2 TNO PRINS MAURITS LAB
H PESKES R IJSSELSTEIN
LANGE KLEIWEG 137
PO BOX 45
2280 AA RIJSWIJK
THE NETHERLANDS
- 6 CENTRE DE RECHERCHES
ET D'ETUDES D'ARCUEIL
D BOUVART C COTTENNOT
S JONNEAUX H ORSINI
S SERROR F TARDIVAL
16 BIS AVENUE PRIEUR DE
LA COTE D'OR
F 94114 ARCUEIL CEDEX
FRANCE
- 1 CDR EUROPEAN RSCH OFFICE
USARDSG (UK)
S SAMPATH
PSC 802 BOX 15
FPO AE 09499-1500